

# Measurement report: Role of Organic Coating and Chemical Composition on Ice Nucleation Potential of Atmospheric Particles in European Arctic

5 Nurun Nahar Lata<sup>1</sup>, Trung Diep<sup>2</sup>, Stefania Gilardoni<sup>3</sup>, Mauro Mazzola<sup>3</sup>, Zezhen Cheng<sup>1</sup>, Ashfiqu  
Rahman<sup>1</sup>, Mickey M. Rogers<sup>1</sup>, Matthew Fraund<sup>4</sup>, Matthew A. Marcus<sup>5</sup>, Naruki Hiranuma<sup>6</sup>, Swarup  
China<sup>1</sup>

<sup>1</sup>Environmental Molecular Sciences Laboratory, Pacific Northwest National Laboratory, Richland, WA, USA

<sup>2</sup>West Texas A&M University, Canyon, TX, USA,

<sup>3</sup>National Research Council –Institute of Polar Sciences (CNR-ISP), Bologna, Italy

10 <sup>4</sup>Fraund Consulting, Inc, Pleasant Hill, CA, USA

<sup>5</sup>Advanced Light Source, Lawrence Berkeley National Laboratory, Berkeley, CA, USA

<sup>6</sup>The University of Texas at El Paso, El Paso, TX, USA

*Correspondence to:* Naruki Hiranuma ([smoon@utep.edu](mailto:smoon@utep.edu)), Swarup China ([swarup.china@pnnl.gov](mailto:swarup.china@pnnl.gov))

**Abstract.** Understanding the ice nucleation (IN) potential of Arctic aerosols is critical for predicting their influence on cloud  
15 formation and water cycles in this vulnerable region. This study investigates the role of particle composition, organic coatings,  
and aerosol sources in modulating ice nucleating particle (INPs) abundance across five aerosol samples collected at the  
Gruvebadet Observatory Station in Ny-Ålesund, Svalbard. The IN potential of Arctic aerosol particles was studied by  
investigating chemical, morphological, and INP abundance measurements. Single-particle analyses revealed distinct  
differences in mixing state, organic volume fraction (OVF), and organic coating morphology across samples. OVF  
20 distributions were linked to particle origin, with marine-influenced Na-rich particles often exhibiting thin organic coatings,  
while long-range transported particles showed thicker organic coatings. Biogenic contributions, though variable, were linked  
to heat-sensitive INPs, suggesting a role for labile biological macromolecules under certain meteorological conditions.  
Spearman rank correlation analysis between particle composition and immersion-mode INP concentrations at two freezing  
temperatures indicated that organic-rich and Na-rich particles were positively associated with enhanced INP abundance.  
25 However, discrepancies in INP abundance were observed for particles with thicker organic coatings, where the morphological  
configuration of the organic material may play a role. The results highlight that Arctic INP variability is governed not only by  
chemical composition but also by the morphological configuration of organic material, which can either enhance or inhibit ice  
nucleation depending on its abundance, distribution, thickness, and mixing state. These findings underscore the combined  
influence of source regions, atmospheric processing, and organic–inorganic interactions in shaping Arctic aerosol freezing  
30 behavior.

**1 Introduction.** The Arctic is undergoing profound and accelerated changes due to environmental change, with surface air  
35 temperatures rising at more than twice the global average, a phenomenon known as Arctic amplification (Forster et al., 2023;  
Screen and Simmonds, 2010; Serreze and Barry, 2011; Wendisch et al., 2019). The interplay of feedback mechanisms,  
including sea ice loss, altered surface albedo, and increased atmospheric moisture, drives these changes, with mixed-phase  
clouds (MPCs) playing a pivotal role in modulating the region's radiative energy balance (Graversen and Wang, 2009;  
Hartmann et al., 2019; Morrison et al., 2005). These clouds, characterized by coexisting supercooled liquid water and ice,  
40 influence both shortwave and longwave radiation, affecting surface temperatures, precipitation, and sea ice dynamics (Korolev  
et al., 2017; Wagner et al., 2021).

Ice-nucleating particles (INPs), a rare subset of atmospheric aerosols, are critical to ice formation in MPCs and thereby impact  
cloud persistence, optical properties, and precipitation efficiency (DeMott et al., 2010; Kanji et al., 2017; Prenni et al., 2007).  
Unlike homogeneous freezing, which requires temperatures below  $-38^{\circ}\text{C}$ , heterogeneous ice nucleation facilitated by INPs  
45 occurs at higher sub-zero temperatures and is strongly dependent on the physicochemical properties of the particles (Hoose  
and Möhler, 2012; Rogers et al., 2001; Vali et al., 2015). These properties, including particle size, morphology, chemical  
composition, and surface characteristics, significantly influence the efficiency and pathways of ice nucleation (Hartmann et  
al., 2019; Knopf et al., 2021; Wagner et al., 2021). For example, larger particles with active surface sites promote ice formation,  
while the presence of organic coatings can either enhance or inhibit nucleation depending on their chemical structure and  
50 interaction with the particle core (Schnell and Vali, 1975; Wilson et al., 2015).

Ice formation in clouds can occur through several heterogeneous freezing modes, including deposition, condensation, contact,  
and immersion freezing. Among these, immersion freezing, where an ice-nucleating particle is immersed within a supercooled  
cloud droplet, is considered the dominant pathway in mixed-phase clouds (MPCs). The sources and variability of INPs in the  
Arctic are influenced by seasonal and environmental factors. During ice-free periods, marine aerosols dominate, often enriched  
55 with organic matter and microorganisms from the sea surface microlayer, which are known to act as effective INPs through  
immersion freezing (Bigg, 1996; Hartmann et al., 2021; Schnell and Vali, 1975; Wagner et al., 2021; Wilson et al., 2015). In  
colder months, long-range transported aerosols, including mineral dust and anthropogenic particles, become significant  
contributors, particularly at temperatures where organic matter is less effective in catalyzing ice formation (DeMott et al.,  
2016; Gong et al., 2020; Li et al., 2022; Rogers et al., 2001). Studies have shown that mineral dust and biogenic aerosols  
60 exhibit distinct ice nucleation efficiencies, with mineral dust typically active at lower temperatures and biogenic particles at  
higher sub-zero temperatures (Augustin-Bauditz et al., 2016; Hartmann et al., 2021; Wagner et al., 2021).

The role of physicochemical properties, such as the composition and mixing state of aerosols, is particularly important in  
understanding their ice nucleation potential. Organic coatings, for instance, can enhance aerosol hygroscopicity and promote  
ice nucleation at moderate freezing temperatures, but they may also block active sites on mineral dust, reducing nucleation

65 efficiency (Augustin-Bauditz et al., 2014; Jahl et al., 2021; Kanji et al., 2019; Knopf et al., 2018; Möhler et al., 2008; Rapp et  
al., 2025; Tang et al., 2016; Xue et al., 2024). Recent studies have increasingly highlighted the importance of surface-active  
biological compounds, particularly proteins and polysaccharides in marine aerosols, which enhance their ice-nucleating  
efficiency under mixed-phase cloud conditions. Laboratory, mesocosm, and field observations demonstrate that these  
macromolecules, often derived from marine fungi, protists, or phytoplankton exudates, contribute significantly to immersion-  
70 mode ice nucleation in the temperature range of -15 °C to -25 °C (Alpert et al., 2022; Hartmann et al., 2021, 2025; Kawana et  
al., 2024; Wagner et al., 2021; Wilson et al., 2015; Zhao et al., 2021). Spectroscopic and modeling studies further confirm that  
these marine exudates drive freezing activity, consistent with holistic parameterizations (Alpert et al., 2022). Aerosol aging  
via oxidation and secondary processing can either enhance or suppress ice nucleation by modifying surface chemistry, phase  
state, and particle structure (Knopf and Forrester, 2011; Xue et al., 2024). Fresh, thin biological coatings from marine organics  
75 may enhance ice formation at warmer temperatures, whereas thick secondary organic layers or organosulfates typically  
suppress nucleation, particularly under cirrus conditions (Rapp et al., 2025; Xue et al., 2024). Laboratory evidence also shows  
that fatty alcohol coatings nucleate ice at significantly warmer temperatures than comparable fatty acid coatings, with strong  
chemical identity and phase-state dependence (Mehndiratta et al., 2024). Aging-induced porosity or glassy transitions in  
secondary organic aerosol can further influence ice-nucleating activity through pore condensation freezing mechanisms  
80 (Wagner et al., 2024).

The variability of INPs and their ice nucleation pathways poses significant challenges for accurately representing Arctic cloud  
processes in climate models. In particular current models often fail to capture the observed seasonal and spatial variations in  
INP concentrations in the Arctic and their resulting influence on cloud phase partitioning and radiative effects (Morrison et  
al., 2005; Storelvmo, 2017; Wagner et al., 2021). Addressing these gaps requires comprehensive measurements of the chemical  
85 composition, size distributions, and ice nucleation properties of Arctic aerosols, particularly under different environmental  
conditions (Hartmann et al., 2021; Korolev et al., 2017; Wilbourn et al., 2024).

This study investigates the chemical composition and ice formation potential of atmospheric particles in the European Arctic,  
with a focus on the role of organic coatings and physicochemical properties. This study couples offline particle composition  
and mixing-state analyses with INP activity measurements to establish links between chemical and morphological properties  
90 with observed freezing behavior. By combining field observations, laboratory analyses, and ice nucleation measurements, this  
work aims to provide new insights into the factors driving ice nucleation in Arctic MPCs and their implications for regional  
and global water cycles.

## 2 Experimental Method

**2.1 Study site, meteorology, and particle sampling:** Aerosol particle and ice-nucleating particle (INP) sampling were  
95 conducted at the Gruevbadet Observatory Station (GVB, 78.918° N, 11.894° E; **Figure S1**) in Ny-Ålesund, Svalbard, from

October 2020 to March 2021. Meteorological parameters, such as relative humidity, temperature, atmospheric pressure, wind speed and wind direction were monitored at the Amundsen-Nobile Climate Change Tower located approximately 1 km NE of GVB (Mazzola et al., 2016) while precipitation data were collected by OTT Pluvio<sup>2</sup> L weighing precipitation gauge (OTT HydroMet GmbH, Kempten, Germany; hereafter Pluvio2) (Ebell et al., 2025) at AWIPEV, Ny-Ålesund, for our campaign  
100 period. The Gruvebadet Observatory is located approximately 1.5 km from the AWIPEV Arctic Research Base in Ny-Ålesund, Svalbard. Precipitation phase/type was determined using a Parsivel<sup>2</sup> optical disdrometer (OTT HydroMet, Germany; hereafter Parsivel2), which measures hydrometeor size and fall velocity (and associated number concentration) to characterize precipitation type and intensity during the aerosol sampling periods. A threshold like  $\leq 0.1$  mm refers to all hydrometeors combined in liquid-equivalent units. Precipitation was measured using an OTT Pluvio<sup>2</sup> L weighing gauge, which reports total  
105 liquid-equivalent precipitation (mm) regardless of hydrometeor phase. Precipitation phase (rain, snow, or mixed) was identified independently using an OTT Parsivel<sup>2</sup> disdrometer.

This study presents the chemical composition and INP concentrations measured offline for particles collected during this period. Aerosol and INP samples were collected throughout the campaign; however, among the available samples, we selected five cases (SA1-SA5) for which collocated samples for single-particle chemical composition and INP analysis were available  
110 (Table 1). A total of 5 pairs of filter samples were collected as part of the Examining INP at GVB (ExINP-GVB) campaign using the same laminar flow stack inlet with the air intake at  $\sim 5$  m above the ground level (Rinaldi et al., 2021). For single particle characterization, aerosol particle sampling was performed using a four-stage Sioutas Cascade Impactor (SKC) with a flow rate of 9 Liters per minute (LPM). The impactor was equipped with TEM grids (Carbon type B film, Ted Pella, Inc) as substrates. To ensure like-for-like comparisons across samples (some of which showed low or no loading on other stages), we  
115 restricted analysis to Stage D (50% cut-off aerodynamic diameter,  $D_{50} = 0.25 \mu\text{m}$ ). All compositional results therefore refer to the Stage-D fraction. Particle sizes reported in this study are based on area-equivalent diameters (AEDs) derived from electron microscopy images and should not be interpreted as aerodynamic diameters. AED does not account for particle density or dynamic shape factor. As a result, particles collected on Stage D ( $D_{50} = 0.25 \mu\text{m}$ ) may exhibit AEDs exceeding the nominal aerodynamic cut-off. This limitation should be considered when interpreting size distributions derived from microscopy.

120 Samples were stored in dark and dry conditions and wrapped with parafilm to prevent photochemical aging. To ensure statistical reliability in single-particle characterization, microscopy and spectroscopy measurements were performed on more than one thousand particles per sample. For offline INP measurements, aerosol particles were collected on 47 mm membrane filters (0.2  $\mu\text{m}$  pore size, Track-Etched Membranes, Whatman) within a total suspended particulate (TSP) inlet at an average flow rate of 5.4 LPM ( $\pm 0.2$  LPM standard deviation) as described in Rinaldi et al. (2021) and Li et al. (2023). Samples were  
125 preserved at  $-20^\circ\text{C}$  immediately after sampling. All ice nucleation measurements in this study were performed offline after sample collection, transport, and cold storage. The validity of this offline analysis approach, including the preservation of heat-sensitive INPs during freezing and transport, is supported by Li et al. (2023), who reported negligible differences between on-site and offline INP measurements for similarly collected Arctic aerosol samples (Li et al., 2023). The analyses were completed

130 within 1 year from the collection of the samples. This approach ensured the detailed characterization of aerosol chemical composition and INP concentrations while maintaining sample integrity throughout the analysis period.

**Table 1.** Sample ID, sampling start and end date, sampled air volume for single particle analysis and ice nucleation.

Samples for Single Particle Analysis				Samples for Ice Nucleation Experiments			
ID	Start Date (UTC)	End Date (UTC)	Sampled Air Volume (L)	ID	Start Date (UTC)	End Date (UTC)	Sampled Air Volume (L)
SA1	10/26/2020 8:30	10/27/2020 13:30	15,660	SA1-INP	10/24/2020 11:15	10/28/2020 13:23	23,707
SA2	1/28/2021 8:14	1/29/2021 7:48	12,726	SA2-INP	1/28/2021 7:52	2/1/2021 8:13	12,726
SA3	2/1/2021 8:03	2/2/2021 13:30	15,903	SA3-INP	2/1/2021 8:16	2/5/2021 9:00	29,290
SA4	2/15/2021 7:53	2/16/2021 7:24	12,699	SA4-INP	2/13/2021 9:15	2/17/2021 8:45	25,687
SA5	3/14/2021 9:53	3/15/2021 9:20	12,663	SA5-INP	3/13/2021 11:55	3/17/2021 10:15	27,501

## 2.2 Back Trajectory of Airmasses

135 To investigate the transport pathways of air masses reaching the measurement site, 48-hour back trajectories were calculated using the Hybrid Single-Particle Lagrangian Integrated Trajectory (HYSPPLIT) model (Rolph et al., 2017; Stein et al., 2015). The analysis was performed using meteorological data from the Global Data Assimilation System (GDAS) with a spatial resolution of  $1^\circ \times 1^\circ$  and a temporal resolution of 3 hours. All trajectories were initiated at 50 meters above ground level, representing the surface layer where interactions with aerosols are most significant. Trajectories were computed every six hours, resulting in eight trajectories per day during the study period. This approach provided a detailed characterization of air mass origins, capturing the temporal variability of transport processes affecting the site. In addition to the back trajectory calculations, a frequency analysis was conducted to identify the dominant transport pathways. Trajectories were overlaid on a  $0.25^\circ \times 0.25^\circ$  spatial grid, and the percentage of trajectories passing through each grid cell was calculated to generate trajectory frequency maps. These maps, categorized into intervals ranging from  $>90\%$  to  $<1\%$ , provide a visual representation of the most frequent air mass routes to the site. This analysis allows for the identification of potential source regions influencing aerosol concentrations at the measurement location, providing important context for interpreting the observed atmospheric

140

145

composition. To assess vertical variability in transport, we also computed height-resolved HYSPLIT back trajectories initialized at 100, 200, and 500 m above ground level (AGL) (Supplementary Information). Trajectories were initiated at near-surface height (50 m AGL) for event classification, and additional trajectories at higher starting altitudes were computed to assess vertical transport variability (Supplementary Information). In addition, the FLEXible PARTicle dispersion model (FLEXPART)(Stohl et al., 2005) was used as a complementary Lagrangian dispersion framework to quantify air-mass residence time and surface-type influence relevant to aerosol transport; the FLEXPART configuration and results are provided in the Supplementary Information. HYSPLIT back trajectories were used here to provide a qualitative characterization of air-mass pathways and potential source regions for event classification, while FLEXPART was applied separately to quantify aerosol residence time, surface-type influence, and free-tropospheric contributions.

155

### 2.3 Single Particle Analysis

We used a computer-controlled scanning electron microscope (CCSEM) to look at single particles (FEI, Quanta 3D). The CCSEM is connected to an energy-dispersive X-ray (EDX) spectrometer with a Si (Li) detector that has an active surface area of 10 mm<sup>2</sup>. The X-ray spectra were taken with a beam current of 0.48 nA and an accelerating voltage of 20 kV. Particle identification was performed using the automated CCSEM/EDX routine, which detects individual particles on the substrate and records an SEM image and an EDX spectrum for each detected particle; the routine also derives geometric properties (e.g., projected area and aspect ratio). CCSEM/EDX particle sizes are reported as projected area-equivalent diameter (AED, m), i.e., the diameter of a circle with the same projected area as the particle. AED is a physical metric and may differ from the impactor's aerodynamic diameter, defined as the diameter of a unit-density sphere with equivalent aerodynamic behavior (Lata et al., 2021, 2023). Only particles with AED between 0.12 and 5 μm were included; smaller particles were excluded because reliable detection and confident EDX spectra could not be ensured. For each detected particle, an EDX spectrum was acquired with 10 s collection time to quantify the relative abundances of 16 elements (C, N, O, Na, Mg, Al, Si, P, S, Cl, K, Ca, Mn, Fe, Zn, and Cu). The reported composition reflects automated multi-location sampling across the particle area rather than a single central spot. The Cu signal in the EDX spectrum is mostly caused by the substrate (copper TEM grids) and the beryllium-copper alloy mounting plate that holds the sample inside the instrument. The CCSEM/EDX data on atomic percentages were then sorted using the rule-based particle classification (Lata et al., 2021). Based on the amount of each element (atomic %), we classified the particles into nine groups: 1) Biogenic 2) Sulfate, 3) Carbonaceous, 4) Dust, 5) carbonaceous mixed dust (Carbonaceous + dust), 6) Sulfate mixed dust (Sulfate + dust), 7) Na-rich ,8) Na-rich sulfate and 9) other. A total of 12,031 particles were characterized with CCSEM/EDX across all the samples. It is important to note that our CCSEM/EDX classification used P and K as tracers of biogenic material, which may not capture the full spectrum of INP-relevant species. In particular, sea surface microlayer (SML)-derived organics and other biogenic components lacking these tracers could be underestimated, and the bulk INP analysis integrates over a broader size range than the stage D particles analysed here. The details of the particle classification scheme are discussed in supplementary **section S1** and **Figure S2**.

175

To investigate the organic characteristics, mixing state of aerosol particles, Scanning Transmission X-ray Microscopy coupled with Near-Edge X-ray Absorption Fine Structure (STXM/NEXAFS) was employed on particles located in substrate regions that were not previously irradiated during CCSEM/EDX analysis, minimizing potential electron-beam-induced damage (Moffet et al., 2010a, b, 2011). STXM/NEXAFS experiments were performed at beamline 5.3.2.2 of the Advanced Light Source, Lawrence Berkeley National Laboratory, and the analysis was performed manually by locating and measuring particles individually (1963 particles total). This synchrotron-based technique scans particles at selected photon energies to produce high-resolution maps of elemental distributions and information on chemical bonding states. The carbon K-edge, spanning photon energies from 278 to 320 eV, was selected to study carbon bonding characteristics within particles. High-resolution spectral ‘stacks’ were recorded at 111 distinct energies, and spatial ‘maps’ were acquired at 11 selected energies. These datasets enabled the identification of different carbon functionalities, including Organic Carbon (OC): Uniformly distributed organic material within particles, Elemental Carbon and Organic Carbon (EC+OC): Particles characterized by sp<sup>2</sup>-hybridized carbon bonds and organic functionalities, Organic-Inorganic Mixtures (OC+IN): Particles with both organic coatings and inorganic cores, and complex mixtures (OC+EC+IN+OC): Particles exhibiting a combination of organic, elemental carbon, and inorganic phases. The images were collected with a spatial resolution of ~30nm and a spectral resolution of ~150meV, enabling detailed examination of particle interiors and surface coatings (Fraund et al., 2019; Kilcoyne et al., 2003). Organic volume fraction (OVF) was determined from STXM/NEXAFS carbon K-edge measurements following the approach of Fraund et al. (2019). Briefly, transmitted-intensity images were converted to optical density and used to separate organic and inorganic contributions within each particle based on the pre-edge and post-edge absorption. OVF was then calculated taking the ratio of organic thickness contribution to the sum of organic and inorganic thickness contribution derived from STXM maps (Fraund et al., 2019, 2020; Knopf et al., 2021; Lata et al., 2021).

#### 2.4 Ice Nucleation Measurements

The WT-CRAFT system, an adaptation of the Cryogenic Refrigerator Applied to Freezing Test (CRAFT) system (Tobo, 2016), was utilized to estimate ambient ice-nucleating particles ( $n_{\text{INP}}$ ) in a unit volume of air from aerosol samples collected at the GVB observatory. The system offers a detection limit of  $>0.001$  INP std L<sup>-1</sup>, enabling the assessment of  $n_{\text{INP}}$  across five samples within a temperature range of -25 to 0 °C, with a systematic uncertainty in freezing temperature of  $\pm 0.5$  °C (Vepuri et al., 2021). Potential background contributions to  $n_{\text{INP}}$  data were significant below -25 °C; hence, the 95% confidence interval was employed to represent experimental uncertainty for each data point (Rinaldi et al., 2021). In each experiment, the freezing properties of 70 droplets (3  $\mu$ L each) were evaluated on a hydrophobic Vaseline layer at a cooling rate of 1 °C min<sup>-1</sup>. Unfrozen droplets were cumulatively counted at intervals of 0.5 °C, with image analysis conducted using ImageJ software for cases where freezing temperatures were ambiguous. Given the negligible background freezing observed in field blank filters at -25 °C (<3%), no background corrections were applied (**Figure S12**). **Table 1** shows a summary of INP sample properties. Sample suspension generation and dilution protocols were executed as per (Rinaldi et al., 2021). Briefly, immediately before freezing analysis, we suspended particles collected on a filter sample in a known volume of ultrapure high-performance liquid chromatography (HPLC) grade water, in which the first frozen droplet corresponded to 0.001 INP std L<sup>-1</sup>, representing our

minimum detection limit. Additionally, heat treatments were performed on all suspensions of atmospheric aerosol samples to study sample composition inferred by INP suppression (Barry et al., 2023). Suspensions were heated at 95 °C for 20 minutes and reanalysed on the WT-CRAFT system to estimate the amount (%) of heat sensitive INPs. The freezing analysis was performed within 24 h after the removal from heat. We want to note that offline particle characterization and immersion-freezing measurements were not performed on identical particle populations with perfectly matched sampling duration and size range; therefore, composition and mixing-state results are interpreted as representative context for each sampling period rather than a direct size-resolved predictor of  $n_{INP}$ . In addition, the droplet freezing assay is conducted on aqueous extracts, and soluble salts and water-soluble organics may dissolve and redistribute during extraction and droplet preparation, potentially modifying surface accessibility compared to the ambient particle state.

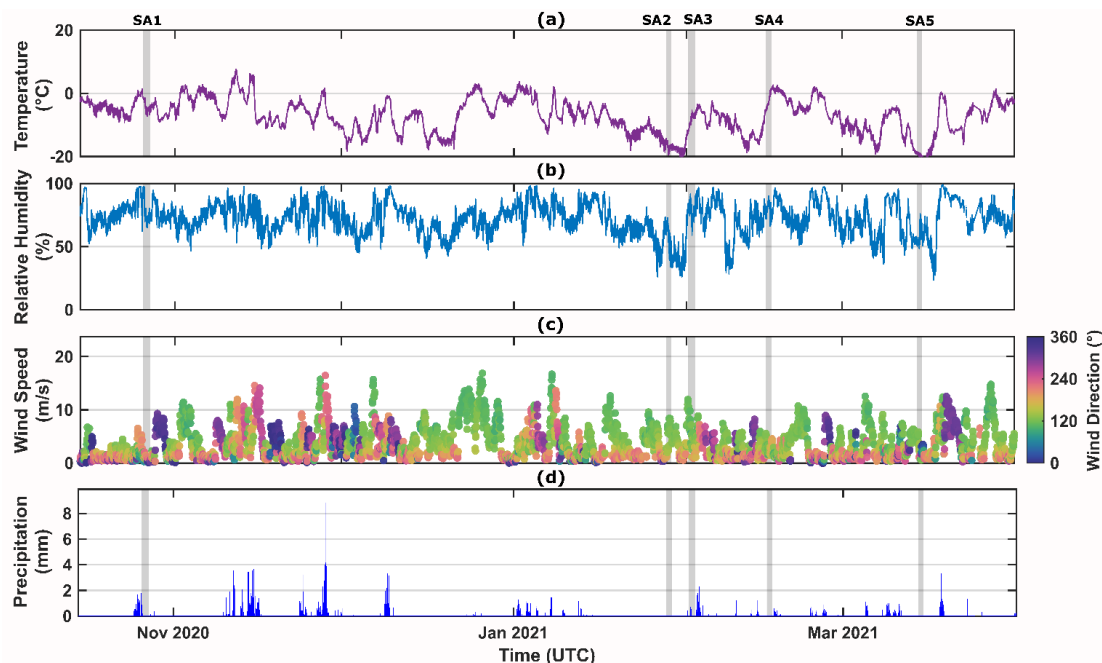


**Figure 1.** Time series of hourly meteorological parameters during the sampling period from November 2020 to April 2021. (a) Temperature (°C), (b) Relative humidity (%), (c) Wind speed (m/s) with wind direction (color scale, °), and (d) Precipitation (mm), all plotted as a function of time (UTC). The shaded regions (SA1 to SA5) indicate the specific time intervals during which particle samples were collected for ice nucleation measurements and single-particle characterization. Zoomed in plots for each sampling time is shown in Supplementary **Figure S5-S9**.

### 3 Results and discussion.

#### 3.1 Meteorological conditions and air mass origin

Synoptic-scale air mass transport governed the local meteorological conditions observed at Ny-Ålesund during each sampling interval (SA1–SA5), as shown in **Figure 1** and summarized in **Table S1**. Key meteorological parameters, including temperature, relative humidity (RH), wind speed, and precipitation exhibited distinct patterns aligned with back trajectory analyses (**Figure 2**), allowing classification of four representative air mass types:

Event 1-SA1 (local/background event): This event is characterized by very low wind speed ( $0.9 \pm 0.7$  m/s) and a mild sub-zero temperature ( $-4.1 \pm 1.5$  °C), SA1 reflects a stagnant local air mass confined within  $\sim 74$ - $79^\circ$ N. Moderate humidity ( $76.4 \pm 9.0$  %) and light precipitation ( $0.05 \pm 0.19$  mm) suggest minimal mixing or transport. This event serves as a background reference dominated by local conditions over the Svalbard archipelago.

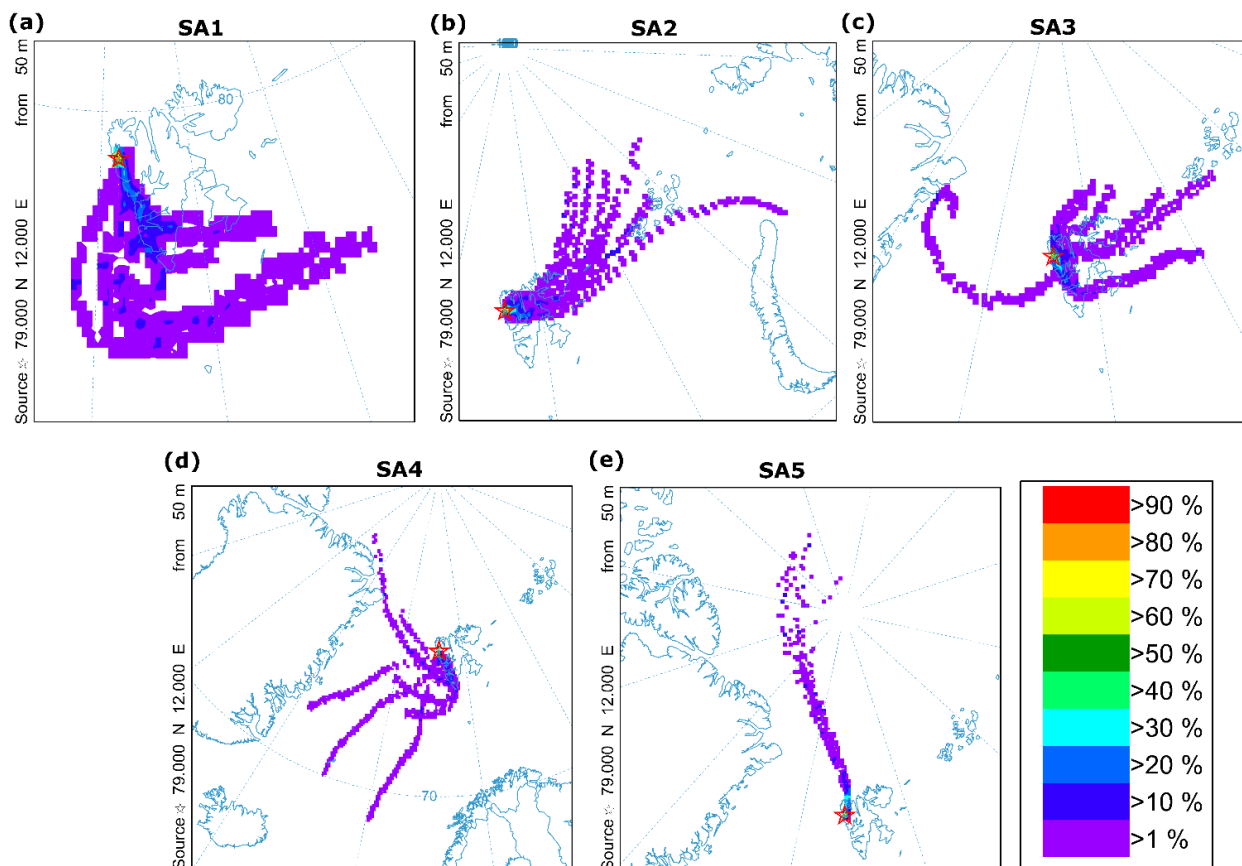


**Figure 2:** HYSPLIT back trajectory frequency maps for air masses arriving at the source location ( $79.00^\circ$  N,  $12.00^\circ$  E) at 50 m above ground level. Panels (a–e) correspond to samples SA1-SA5 and illustrate the origins and transport pathways of air parcels during the respective sampling periods. The color scale represents the percentage of trajectories passing through each grid cell, with cooler colors (purple/blue) indicating lower frequencies and warmer colors (yellow/red) indicating higher frequencies. All panels use the same frequency scale shown on the right. The red star indicates the sampling location.

Event 2-SA2 and SA5 (cold high-latitude Arctic events): These events were marked by cold, dry, and moderately windy conditions, with temperatures of  $-16.7 \pm 0.9$  °C and  $-19.5 \pm 0.6$  °C, RH around 57-59 %, and wind speeds of  $4.9 \pm 2.9$  m/s (SA2) and  $3.0 \pm 1.9$  m/s (SA5). Both occurred under zero precipitation. HYSPLIT analysis shows air mass transport from the high Arctic ( $>80^\circ$ N), consistent with classic Arctic cold-air outbreak regimes.

Event 3-SA3 (northwest mixed event): Intermediate in temperature ( $-8.4 \pm 1.7$  °C), with elevated RH ( $78.3 \pm 6.6$  %) and the highest wind speed among all periods ( $5.6 \pm 3.0$  m/s), SA3 reflects a dynamically mixed air mass arriving from northwestern directions. Light precipitation ( $0.09 \pm 0.20$  mm) coincided with comparatively high wind speed, suggesting stronger boundary layer exchange than in other periods.

Event 4-SA4 (eastern warm-moist intrusion): SA4 was associated with air masses originating from latitudes south of  $70^{\circ}\text{N}$ , bringing the distinctly warmest ( $-2.2 \pm 2.3$  °C) and most humid ( $79.1 \pm 6.2$  %) conditions. Wind speeds remained low ( $2.8 \pm 1.4$  m/s), and precipitation was negligible ( $0.00 \pm 0.02$  mm). This synoptic setup reflects a mid-latitude intrusion, likely leading to enhanced atmospheric processing and particle ageing during transport. Although we cannot isolate the dominant ageing mechanism without concurrent gas-phase or radiation measurements, the warm and humid intrusion pathway implies greater cumulative exposure during transport (e.g., longer time for ageing and potential interaction with more reactive lower-latitude air masses and cloud processing along the pathway). Such conditions are consistent with findings by Raif et al. (2024), which associate elevated INP concentrations with aged aerosols transported from lower-latitude continental regions (Raif et al., 2024). To evaluate endpoint-height sensitivity and wet removal prior to arrival, we additionally report 120 h height-resolved trajectories (100-500 m AGL) and trajectory-accumulated precipitation in the Supplementary Information (**Figure S11-S12**)

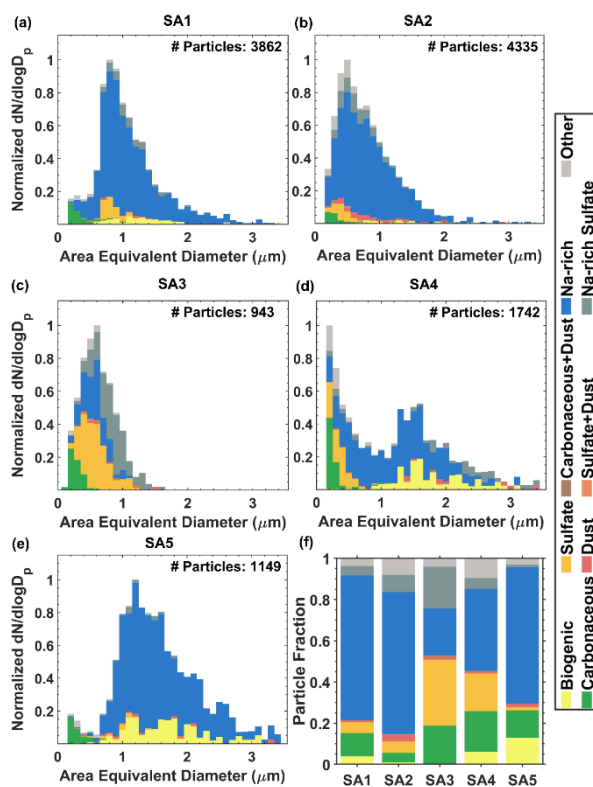


**Figure 3:** (a-e) Size-resolved particle classes obtained from CCSEM/EDX for five samples. Number indicates the total number of particles analysed for each of the samples. (f) the normalized particle fraction of each of the classes for five samples.

### 265 3.2 Single particle composition from CCSEM/EDX and STXM/NEXAFS

**Figure 3** provides insights into the size-resolved chemical composition of aerosol samples (SA1-SA5) derived from CCSEM/EDX, revealing variations in particle classes linked to meteorological conditions and air mass histories (**Figures 1-2**). STXM/NEXAFS data in **Figure 4** further support these trends by resolving the internal chemical mixing states of individual particles. SA1, representing a stagnant local event, was dominated by Na-rich particles ( $73.6 \pm 0.7\%$ ), with moderate contributions from OC+In ( $52.4 \pm 1.0\%$ ) and OC+In+EC ( $28.4 \pm 1.2\%$ ). Despite low wind speeds and minimal vertical mixing, black carbon inputs from domestic (30.86%) and flaring (18.56%) sources were detected (**Table S3 and Figure S3**), but the overall particle population likely reflects fresh marine aerosol mixed with locally emitted organic material. The presence of biogenic particles (3.9%) indicates potential influence from nearby coastal ecosystems and marine biota. These findings align with prior observations of unprocessed sea spray aerosols in Svalbard during calm conditions (Bigg, 1996; Leck and Svensson, 2015), and marine biogenic sources of INPs under low turbulence (Wilson et al., 2015).

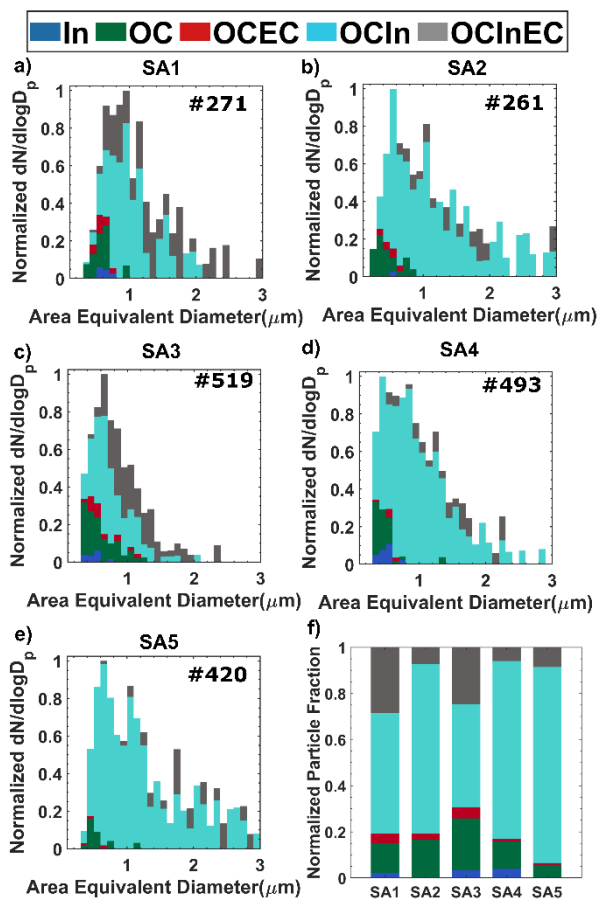
SA2 and SA5, both influenced by high-latitude Arctic air masses, were dominated by Na-rich particles ( $69.0 \pm 1.2\%$  and  $66.2 \pm 1.0\%$ , respectively), but exhibited contrasting signatures of atmospheric processing. SA2 showed higher fractions of Na-rich sulfate ( $8.2 \pm 0.4\%$ ) and sulfate ( $6.4 \pm 1.0\%$ ), coupled with a lower percentage of OC+In+EC ( $11.4 \pm 0.6\%$ ), indicative of chemical aging during long-range transport. These air masses spent substantial time in the free troposphere (80.8%) and over closed ice surfaces (11.4%), conditions conducive to the oxidation of sulfur precursors and subsequent sulfate formation (Gong et al., 2020; Huang et al., 2018; Quinn et al., 2002).

In contrast, SA5, influenced by high-latitude Arctic air masses, displayed a chemical and mixing state signature indicative of limited atmospheric aging. The CCSEM/EDX results showed a dominant Na-rich particle fraction ( $78.2 \pm 1.0\%$ ) with negligible sulfate components, while the STXM/NEXAFS analysis revealed an exceptionally high proportion of OC+In particles ( $85.0 \pm 1.7\%$ ). The fraction of OC+EC particles was notably low ( $0.7 \pm 0.4\%$ ). However EC can arise from multiple combustion sources, in the European Arctic during late winter and early spring. The scarcity of such mixtures (low OC+EC), together with negligible sulfate, suggests a lack of significant anthropogenic influence. Importantly, this interpretation is supported not only by mixing-state evidence but also by FLEXPART back trajectory analysis (**Table S3; Figure S3**), which showed that SA5 air masses spent most of their history over cryospheric and marine regions with minimal exposure to continental or industrial source areas. The relatively high abundance of biogenic particles (12.8%) and the dominance of Na-rich class from CCSEM/EDX and OC+In mixing states from STXM/NEXAFS therefore point toward natural cryospheric and marine contributions, consistent with prior observations of biological and organic material emissions from sea ice and snowpack surfaces (Baccarini et al., 2020; Beck et al., 2021; Gong et al., 2023), although the ice-nucleating potential of such particles remains an active area of investigation (Wagner et al., 2021).

SA3, under north-westerly mixed conditions with the highest wind speed ( $5.6 \pm 3.0$  m/s), presented the most processed chemical signature. It had the highest sulfate ( $28.5 \pm 1.5\%$ ) and Na-rich sulfate ( $11.2 \pm 1.2\%$ ) fractions, along with a high fraction of OC+In+EC particles ( $24.7 \pm 1.0\%$ ). This composition indicates anthropogenic input likely from flaring (22.78%) and industrial sources (11.92%) (**Table S3 and Figure S3**) in northern Europe and Russia, transported into the Arctic boundary

layer. FLEXPART-BC (**Figure S3**) indicate near-background aerosol mass during SA3, the prevalence of sulfate and Na-rich sulfate (often occurring as internally mixed particles), together with the transport pathways, suggests the influence of long-range transported, aged aerosols of predominantly anthropogenic origin. Enhanced particle heterogeneity, including sulfate and Na-rich-sulfate mixtures, suggests active secondary aerosol formation and mixing hallmarks of Arctic haze events during late winter and early spring (Quinn et al., 2002; Schmale et al., 2022; Tunved et al., 2013). Such aged particles are known to modulate both cloud condensation and ice nucleation properties (Creamean et al., 2018; Hiranuma et al., 2013).

SA4, influenced by a warm and moist air mass originating from south of 70°N, exhibited a chemical composition with Na-rich ( $43.9 \pm 0.9\%$ ), sulfate ( $15.9 \pm 1.2\%$ ), and carbonaceous ( $22.7 \pm 1.3\%$ ) particles and a notable biogenic particle fraction (6.1%). The elevated organic content and dominance of OC+In ( $77.1 \pm 1.9\%$ ) suggest substantial presence of organics in marine aerosols without strong elemental carbon (OC+In+EC:  $6.0 \pm 0.8\%$ ). FLEXPART trajectories indicate that this air mass spent approximately 11% of time over open water (**Table S3** and **Figure S3**), likely facilitating the entrainment of marine biogenic matter and promoting partial chemical transformation. These observations are consistent with previous Arctic studies linking moist mid-latitude intrusions to marine organic enrichment and enhanced INP concentrations (Hartmann et al., 2021; Wilson et al., 2015). The absence of strong industrial or biomass burning signatures suggests that natural marine and coastal ecosystems were the dominant aerosol sources during this event.



315 **Figure 4:** Chemical mixing state of individual particles collected at different periods. (a-e) Distribution of analysed particles measured by STXM/NEXAFS. (f) Normalized fractions of different classes of internally mixed particles for different samples are shown.

### 3.3 Ice Nucleation properties

320 **Figure 5** displays the temperature-dependent INP number concentrations,  $n_{\text{INP}}(T)$ , for aerosol samples SA1-SA5 and their response to heat treatment. At  $-15\text{ }^{\circ}\text{C}$ , untreated  $n_{\text{INP}}$  ranged from  $0.001$  to  $0.004\text{ L}^{-1}$  ( $0.003 \pm 0.001\text{ L}^{-1}$ ; **Figure 5a-e**). At  $-25\text{ }^{\circ}\text{C}$ ,  $n_{\text{INP}}$  increased by approximately two orders of magnitude to  $0.27 \pm 0.06\text{ L}^{-1}$ , with a relatively narrow inter-sample range ( $0.20\text{-}0.34\text{ L}^{-1}$ ). The temperature range from  $-15\text{ }^{\circ}\text{C}$  to  $-25\text{ }^{\circ}\text{C}$  is important for comparison to previous Arctic INP measurements due to its relevance for Arctic mixed-phase clouds (Morrison et al., 2012). Overall, the  $n_{\text{INP}}(T)$  spectra show similar temperature dependence across samples, whereas heat sensitivity differs substantially. Using a conservative detection-limit substitution for heated spectra (**Section S5**), the mean heat-labile fractions (mean  $\pm$  SD across temperatures) are  $76 \pm 19\%$  (SA1),  $54 \pm 30\%$  (SA2),  $37 \pm 33\%$  (SA3),  $54 \pm 34\%$  (SA4), and  $48 \pm 30\%$  (SA5) (**Figure 5f-j**). The measured amount of heat-labile and heat-stable INPs (%) as a function of temperature suggests the source(s) of INPs including biogenic or organic

325

material such as proteins from certain species of bacteria and fungi active at temperatures up to and warmer than  $-15\text{ }^{\circ}\text{C}$ , mineral dust that is efficient below about  $-20\text{ }^{\circ}\text{C}$ , and complex organics that are effective over the entire temperature range (e.g., Hill et al., 2017; J. Murray et al., 2012; Knopf et al., 2018). A similar range of ambient  $n_{\text{INP}}$  measured in this study has been previously found in European Arctic regions (Creamean et al., 2022; Irish et al., 2019a; Li et al., 2023; Rinaldi et al., 2021; Welti et al., 2020). Creamean et al. (2022) reported  $<0.1\text{ L}^{-1}$  at  $-25\text{ }^{\circ}\text{C}$  during the Multidisciplinary drifting Observatory for the Study of Arctic Climate (MOSAiC) expedition in the Central Arctic (September 2019 - October 2020). Similar to the Creamean et al. (2022), the offline freezing assay performed by Welti et al. (2020) during the PASCAL campaign, conducted aboard the research vessel Polarstern (expedition PS106) in the vicinity of Svalbard, Norway (May-July 2017), measured INP concentrations at  $-28\text{ }^{\circ}\text{C}$  that were limited by the detection threshold of the droplet freezing assay (Welti et al., 2020). Continental dust during winter and marine biota from ice-free open water in summer were identified as the potential INP sources (Creamean et al., 2019, 2022; Irish et al., 2019a, b). Rinaldi et al. (2021) reported offline INP concentrations from samples collected at a ground-based site near Ny-Ålesund between April and August 2018, providing site-relevant context for comparison (Rinaldi et al., 2021). Their highest INP concentrations were lower than those reported for the Arctic Cold Air Outbreak (ACAO) campaign and were typically 1-3 orders of magnitude below those measured in this study (Raif et al., 2024). Similarly, Li et al. (2023) reported Ny-Ålesund INP concentrations during October-November 2019 using offline droplet-freezing measurements on filter samples; these values were generally 1-4 orders of magnitude lower than those reported for the ACAO campaign (Li et al., 2023; Raif et al., 2024).

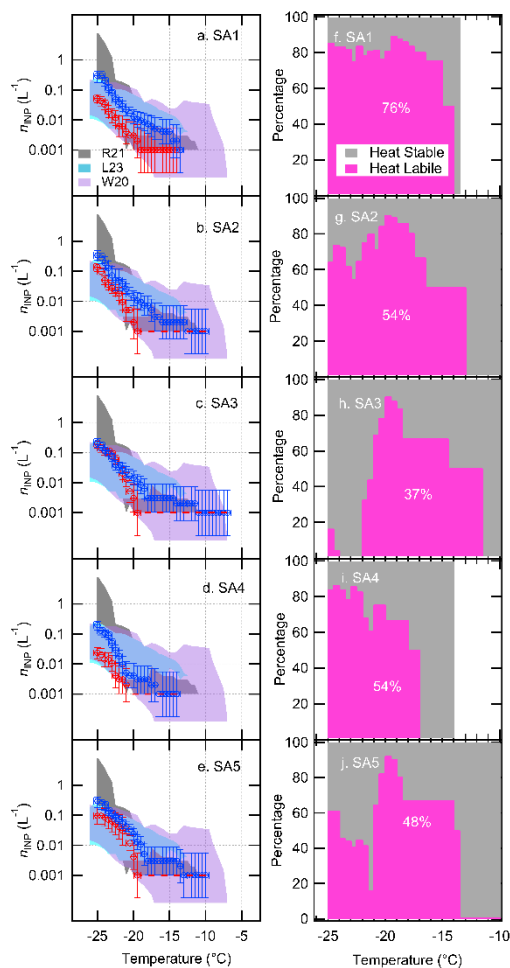
Despite small inter-sample deviation in  $n_{\text{INP}}$  at the examined freezing temperatures, the samples exhibit distinctly different heat sensitivities. Across SA1-SA5, heating reduces  $n_{\text{INP}}$  most clearly at warmer temperatures (approximately  $-15$  to  $-20\text{ }^{\circ}\text{C}$ ), indicating that a substantial fraction of INPs is heat-labile, while differences among samples are more strongly expressed in their heat-labile versus heat-stable partitioning than in  $n_{\text{INP}}$  magnitude alone. Given the limited sample size ( $n = 5$ ), the heat-labile signatures are interpreted as evidence for contributions from labile organic/biological INPs, potentially including marine-derived material, rather than as definitive proof of a specific source such as the sea surface microlayer (SML). SA2 and SA4 show similar mean heat-labile fractions ( $\sim 54\%$  each; **Figure 5g, i**) and  $n_{\text{INP}}$  values near  $-25\text{ }^{\circ}\text{C}$  that remain within the overall inter-sample range, while their warmer-temperature  $n_{\text{INP}}$  is broadly comparable to the other samples. SA2 and SA4 contain 16.1% and 12.0% OC-rich particles (STXM/NEXAFS), respectively, supporting an appreciable organic contribution. For SA2, under cold conditions ( $-16.7\text{ }^{\circ}\text{C}$ ,  $\text{RH} \approx 57\%$ ), the combination of a high OC+IN fraction (73.6%, STXM/NEXAFS), a high Na-rich particle fraction ( $\sim 69\%$ , CCSEM/EDX), and a moderate heat-labile response is consistent with INPs associated with organic/biological material internally mixed with Na-rich particles (DeMott et al., 2016; Hoose and Möhler, 2012; Ickes et al., 2020; Irish et al., 2019b). In contrast, SA4 despite warmer, relatively more humid conditions ( $-2.2\text{ }^{\circ}\text{C}$ ,  $\text{RH} \sim 79\%$ ) and high residence over open water (11%) also shows substantial INP concentration ( $n_{\text{INP}}$ ) and heat sensitivity. This behavior is consistent with the presence of biogenic particles (6.1%) together with abundant Na-rich particles and possible influences of atmospheric aging/secondary processing during mid-latitude intrusions, which can modify organic-inorganic mixing and

apparent freezing efficiency (Christiansen et al., 2020; Kirpes et al., 2019; Wilson et al., 2015). Thus, while their dominant particle classes differ, both SA2 and SA4 indicate coupled organic/biogenic and inorganic (Na-rich) contributions to the observed INP populations. Contributions from mineral dust acting as a carrier for biological INPs are unlikely to dominate, as CCSEM/EDX analysis shows only a minor dust fraction in SA4 (**Figure 3**).

365 Interestingly, SA3 and SA5, influenced by cold and dry Arctic air masses, exhibit significant  $n_{\text{INP}}$  only below  $-20\text{ }^{\circ}\text{C}$ , with minimal reduction after heat treatment, indicating the predominance of heat-stable INPs. This trend is consistent with the presence of mineral dust, NaCl, and non-biological heat-stable organics (Chi et al., 2015; Knopf and Forrester, 2011; Patnaude et al., 2024). In SA3, despite high pre-heating  $n_{\text{INP}}$ , a measurable reduction after heat treatment (mean heat-labile fraction  $\approx 37\%$ ; **Figure 5h**), together with elevated sulfate (32.1%), Na-rich sulfate (20.2%), and carbonaceous particles (18.7%), points  
370 to internally mixed and processed aerosol populations potentially involving marine-influenced material and long-range transported organics, a combination shown to modify freezing efficiency (Knopf and Forrester, 2011; Mirrielees et al., 2024). In contrast, SA5, although displaying the highest biogenic particle fraction (12.8%), shows only moderate  $n_{\text{INP}}$  and a mixed heat response (mean heat-labile fraction  $\approx 48\%$ ; **Figure 5j**), indicating that a substantial portion of INPs are heat-stable within the examined temperature range rather than being fully heat-insensitive. This counterintuitive observation suggests that not all  
375 biogenic particles are equally ice-active at given freezing temperatures, possibly due to the presence of non-IN-active biological debris, such as fragmented cells or detritus, or the deactivation of active sites by coatings from secondary organic or inorganic species (DeMott et al., 2010; Kirpes et al., 2019). These results highlight the importance of particle mixing state and chemical processing in modulating INP activity, even among biogenic aerosol fractions.

Meanwhile, SA1, characterized by marine influence and more humid conditions, shows a strong heat response (mean heat-labile fraction  $\approx 76\%$ ; **Figure 5f**), with  $n_{\text{INP}}$  at warmer temperatures (around  $-15\text{ }^{\circ}\text{C}$ ) decreasing markedly upon heating, indicating a substantial contribution from heat-labile INPs. Such INPs are consistent with proteinaceous or other labile biological material that can be enriched in the sea surface microlayer (SML), rather than heat-resistant polysaccharidic INPs (Christiansen et al., 2020; Hartmann et al., 2025; Jayaweera and Flanagan, 1982; Wilson et al., 2015). The high abundance of Na-rich particles (70.3%) together with substantial OC and OC+In fractions suggests Na-rich particles internally mixed with  
385 organics and biological material, consistent with enrichment from the SML. Several studies have demonstrated that sea spray aerosol enriched in organic matter from the SML (especially polysaccharides and proteinaceous compounds) can serve as immersion-mode INPs in mixed-phase clouds (DeMott et al., 2016; Wilson et al., 2015; Zhao et al., 2021). This supports our interpretation that particles with high OC and OC+In fractions in SA1 (coated sea salt with biogenic components) are plausible contributors to heat-labile INP activity. Collectively, these observations demonstrate that IN property is not solely dependent  
390 on particle source (e.g., biogenic vs. inorganic), but also on the particle mixing state, and atmospheric processing influencing the ice-nucleating potential (Hartmann et al., 2021; Hoose and Möhler, 2012; Ickes et al., 2020). Precipitation influence on INP abundance and composition during the sampling periods is likely minimal, as site precipitation was dry or very low ( $\leq 0.1$

mm; **Table S1**) and trajectory-based accumulated precipitation was negligible (**Figure S11**), indicating limited wet scavenging prior to arrival.



395

**Figure 5.** Immersion freezing of the particle samples collected at different time periods. In Panels (a)-(e), the blue circles indicate the ambient number concentration of INPs before heat treatment, and the red circle indicates the INP number after heat treatment. Red dashed lines show the lowest detection limit of  $n_{INP}$  for this study. Color-shaded areas show the previous results of INP measurements from GVB via the same freezing assay (Rinaldi et al., 2021; Li et al., 2023), as well as from the PS 106 Arctic expedition in the vicinity of Svalbard, Norway (May – July 2017; Welti et al., 2020). Panels (f)-(j) show the amount of heat-labile and -stable INPs (%) for SA1-SA5. We use the lowest detectable  $n_{INP}$  (i.e.,  $0.001 L^{-1}$ ) for  $n_{INP,heated}(T)$  in the case there were no measured values for freezing temperatures, in which  $n_{INP,untreated}(T)$  was measured.

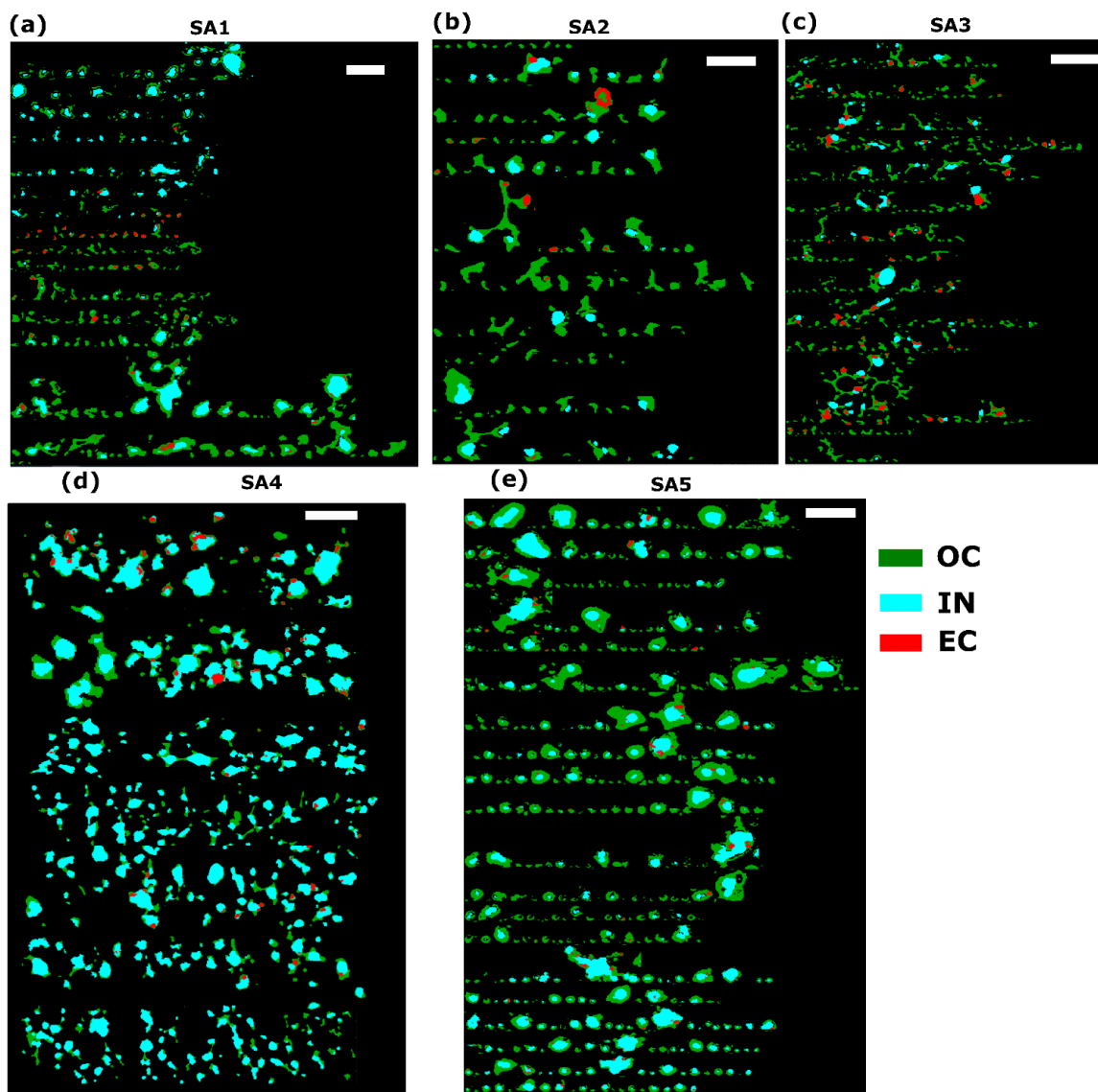
400

### 3.4 Effect of organic coating and organic volume fraction on ice nucleation

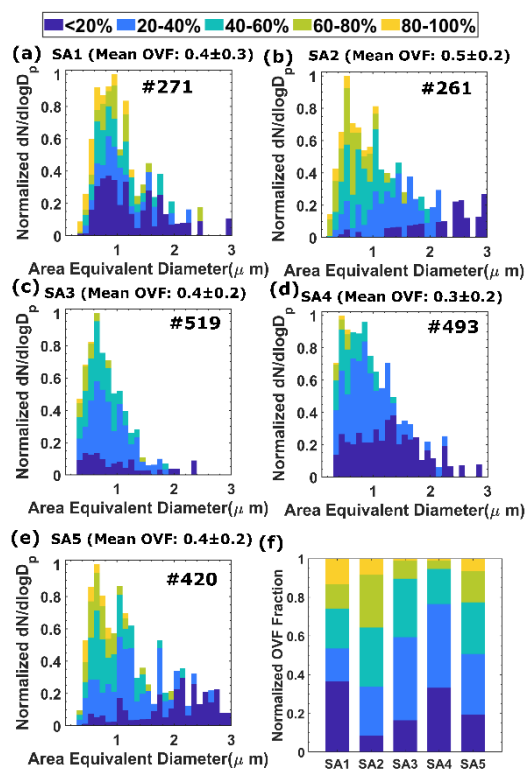
To assess the impact of organic coatings and the organic volume fraction (OVF) on the ice nucleation potential of ambient Arctic aerosol particles, we examined the STXM/NEXAFS-derived mixing state and OVF bin distributions (**Figure 6** and

405

410 **Figure 7**), and their correlations with INP concentrations at two freezing temperatures (**Figure 8**). The two freezing temperatures, -14 °C and -24 °C, were selected to represent a moderate and a colder regime of immersion freezing, respectively, and because INP concentration data was available at both points to allow statistical analysis. The organic volume fraction was categorized into bins of <20%, 20–40%, 40–60%, 60–80%, and 80–100%. Samples with a high proportion of particles in the 60–80% and 80–100% bins were considered organic-rich; those in the 40–60% range were defined as moderate; 20–40% as low; and <20% as the lowest in organic content (Knopf et al., 2021).



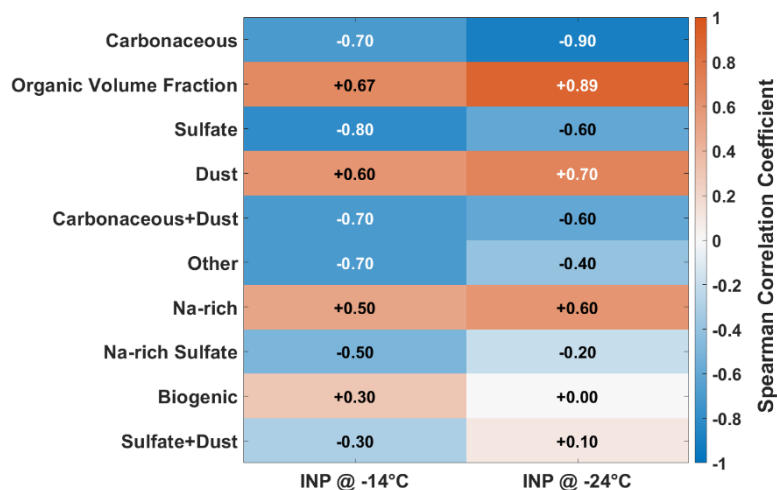
415 **Figure 6:** Carbon speciation maps of each of the particle samples. Colors correspond to experimentally defined chemical components; green indicates organics (OC), red- elemental carbon (EC), and teal indicates inorganic (IN) rich region. Note that each pixel can contain up to three components resulting in overlapping colors. Here each of the scale bar indicates 1  $\mu\text{m}$ .



420 **Figure 7:** The organic volume fraction of individual particles collected at different time periods. (a-e) Distribution of analysed particles measured by STXM/NEXAFS from ground to different altitudes. Panel (f) shows the fractions of different OVF-containing particles at different times are shown. The number (#) inside each plot indicates the total number of particles analysed for each of the samples.

425 As shown in **Figure 7** and the tabulated results (**Table S2**), SA2 and SA5 contain the highest fractions of organic-rich particles (27.2 % and 16.2 % in the 60–80 % bin, respectively), while SA1 and SA3 contain a majority of low (<20 %) and low-moderate (20–40 %) OVF particles. SA4 has the lowest overall OVF ( $0.3 \pm 0.2$ ) and minimal contribution from high-OVF bins, indicating a less organic-rich character. This classification is consistent with the overall OVF values: 0.5 for SA2, 0.4 for SA1, SA3, and SA5, and 0.3 for SA4. This gradation in organic volume fraction (OVF) is reflected in the Spearman rank correlations between OVF and INP concentrations (**Figure 8**), which show moderate to strong positive relationships ( $\rho = 0.67$  at  $-14^\circ\text{C}$  and  $\rho = 0.89$  at  $-24^\circ\text{C}$ ). These correlations indicate that samples enriched in organic material, particularly those dominated by higher OVF bins (60–100%), tend to exhibit higher INP concentrations under both moderately supercooled ( $-14^\circ\text{C}$ ) and colder ( $-24^\circ\text{C}$ ) conditions. This behavior is consistent with previous studies demonstrating the importance of organic-rich particles

430 and organic coatings for immersion freezing, either through intrinsic biological ice-nucleating material or through modification of particle surface properties (Augustin-Bauditz et al., 2014; Ickes et al., 2020; Kanji et al., 2019; Wilson et al., 2015).



435 **Figure 8.** Spearman rank correlation coefficients between ice-nucleating particle (INP) concentrations and particle composition metrics (number fraction in each sample) at two freezing temperatures, -14 °C (left) and -24 °C (right), prior to heating. Each row represents a particle class or metric, including biogenic, carbonaceous, sulfate, dust, mixed types (e.g., carbonaceous + dust), Na-rich categories, and organic volume fraction (OVF). Orange/red shading indicates positive correlations and blue shading indicates negative correlations, with lighter colors indicating values closer to zero.

In addition to OVF, several particle classes derived from CCSEM/EDX exhibited temperature-dependent associations with INP concentrations. Biogenic and Na-rich particles showed weak to moderate positive correlations ( $\rho = 0.30$  and  $0.50$  at -14 °C;  $\rho = 0.00$  and  $0.60$  at -24 °C), suggesting a potential contribution from marine-influenced organic material, particularly at colder temperatures. These trends align with the findings in **Section 3.3**, where heat-sensitive INPs were associated with biological and organic contributions (DeMott et al., 2010; Hartmann et al., 2021; Kawana et al., 2024; Zhao et al., 2021). Despite SA5 having the highest biogenic fraction (12.8 %) and OCIn fraction (85 %), its  $n_{\text{INP}}$  is moderate compared to SA2 and SA4. This discrepancy can be explained by the STXM-derived compositional maps (**Figure 6e**), which show that SA5 particles are coated with thick organic layers. These thick coatings may cause a shielding effect where the organic coating potentially masks the ice-active sites, lowering nucleation efficiency (Knopf et al., 2018; Rapp et al., 2025; Tang et al., 2016; Xue et al., 2024). In contrast, carbonaceous and sulfate particles displayed moderate to strong negative correlations with INP concentrations at both temperatures, indicating that these particle types are less efficient INPs in this dataset. Dust exhibited positive correlations with  $n_{\text{INP}}$  at both temperatures ( $\rho = 0.60$  at -14 °C and  $\rho = 0.70$  at -24 °C), despite representing a minor fraction of the particle population based on CCSEM/EDX analysis. Given the small sample size ( $n = 5$ ) and low dust abundance, this relationship should be interpreted cautiously and is considered exploratory.

In contrast, SA2, although low in biogenic content (0.9 %), exhibits high INP abundance and a high OCIn fraction (73.6 %). The STXM maps (**Figure 6b**) visually show thinner organic coatings, allowing better access to active sites or possibly promoting heterogeneous freezing via organic-induced deliquescence or restructuring. While our measurements do not directly  
455 resolve the freezing pathway, organic coatings can plausibly influence heterogeneous freezing by modifying particle water uptake and phase state. For example, transitions between liquid and highly viscous/glassy organic phases can limit water diffusion and alter when and how an underlying ice-active surface becomes accessible, which can change the apparent freezing efficiency (Berkemeier et al., 2014; Schill and Tolbert, 2013; Zobrist et al., 2008). In addition, organic coatings and internal  
460 deliquescence and ice formation under cold, humid conditions (Möhler et al., 2008; Schill and Tolbert, 2013). This suggests that organic material internally mixed with inorganics can significantly enhance  $n_{\text{INP}}$  through favorable surface or interfacial properties (Hartmann et al., 2025; Knopf and Forrester, 2011; Wagner et al., 2021; Wilson et al., 2015). SA4 presents an intriguing case: despite having the lowest overall OVF and minimal high-OVF fraction, it displays strong  $n_{\text{INP}}$  and heat sensitivity. As observed in the STXM image (**Figure 6d**), the organic coatings appear relatively thin and patchy. This organic  
465 coating distribution, combined with its moderate biogenic content (6.1 %) and marine influence, may facilitate  $n_{\text{INP}}$  through partial organic coverage that still exposes active sites, possibly enriched with surface-active polysaccharides and proteins from the sea surface microlayer (Alpert et al., 2022; Christiansen et al., 2020; Kirpes et al., 2019; Wilson et al., 2015). Overall, these results highlight that not only the presence of organic material but also its distribution (geometry), thickness, and mixing state critically influence ice nucleation. Thick coatings may suppress activity, while thinner or patchy organic layers can enhance it  
470 depending on the physicochemical composition.

#### 4 Summary and conclusion

This study examined the ice nucleation potential of Arctic aerosols by integrating single-particle chemical composition, mixing state, organic volume fraction (OVF), and spatial distribution of organic coatings with air mass back trajectory analysis and  $n_{\text{INP}}$  measurements. Our results indicate that differences in freezing behavior across samples are associated with variations in  
475 particle composition and organic coating characteristics. Observed associations include higher  $n_{\text{INP}}$  in some samples containing Na-rich particles with thinner organic coatings and, in certain cases, biogenic particles. However, these relationships are not consistent across all samples or conditions. Instead, the observations point to a complex interplay between chemical composition, morphological configuration of coatings, and meteorological influences, where multiple particle types and surface properties may contribute to immersion freezing in the Arctic atmosphere.

480 Aerosols enriched in Na-rich particle types with relatively thin organic coatings showed moderate  $n_{\text{INP}}$  prior to heat treatment. However, the most direct indicator of biological (heat-sensitive) contributions is the temperature-dependent reduction in  $n_{\text{INP}}$  after heating, rather than Na-rich composition alone. Across the five samples, the heat-labile fraction varies substantially, while

heat-stable INPs dominate at colder temperatures. Overall, these results indicate that Arctic  $n_{\text{INP}}$  reflects the combined influence of particle composition, coating distribution/mixing state, and air-mass history, with the relative importance of heat-labile  
485 versus heat-stable INPs depending on temperature regime.

This study provides initial insights into the how organic coatings, aerosol composition, and source contributions influence the role of Arctic aerosols in modulating cloud formation processes in one of Earth's most vulnerable regions. Future studies should aim to validate these findings using laboratory experiments, and more field-collected samples and incorporate these mechanistic insights into Earth system models to better predict the implications of aerosol freezing on Arctic cloud dynamics  
490 and water cycles. Our results show that (1) mixed and aged aerosols in warm and moist air mass contain high sub-zero temperature INPs active at warmer than  $-15\text{ }^{\circ}\text{C}$  and (2) the heat sensitivity of INPs depends on aerosol composition and sources (i.e., the more mineral aerosols include, the more heat-stable INPs are). Due to current pan-Arctic warming trends, substantial changes in the Arctic landscape (Murray et al., 2021) such as more open water and land exposure to air, will influence ambient aerosol mixing processes and warm air intrusion to high-Arctic in the future.

#### 495 **Data availability**

The supporting text, figures, and tables are available in the Supplement. Experimental data have been deposited in open-access data repository (<https://doi.org/10.5281/zenodo.17373230>).

#### **Author contributions**

NNL, NH, SG and SC conceptualized the study and designed the experiments. NNL wrote the original manuscript and  
500 performed the CCSEM/EDX analysis and led the STXM/NEXAFS analysis. SG and MM conducted particle sampling. TD performed the ice nucleation experiments. AR, ZC, and MMR collected the STXM data, and MF and MAM supported STXM/NEXAFS data acquisition. TD and NH contributed to the interpretation of the ice nucleation results. All authors reviewed and edited the manuscript.

#### **Competing interests**

505 Some authors are members of the editorial board of journal ACP. (Stefania Gilardoni is an editorial board member).

#### **Acknowledgement**

This material is based upon work supported by the National Science Foundation under grant no. 1941317. Some of this research was funded using project award (10.46936/expl.proj.2023.61007/60012354), using resources at the Environmental Molecular Sciences Laboratory (EMSL), which is U.S. Department of Energy (DOE) Scientific User Facilities. EMSL is sponsored by  
510 the Office of Biological and Environmental Research (OBER) and operated under Contract Nos. DE-AC05-76RL01830. This

research used resources of the Advanced Light Source, a U.S. DOE Office of Science User Facility under contract no. DE-AC02-05CH11231. We thank Kerstin Ebell from University of Cologne for sharing Pluvio data. The authors used Grammarly solely for grammar and language editing.

## References

- 515 Alpert, P. A., Kilhau, W. P., O'Brien, R. E., Moffet, R. C., Gilles, M. K., Wang, B., Laskin, A., Aller, J. Y., and Knopf, D. A.: Ice-nucleating agents in sea spray aerosol identified and quantified with a holistic multimodal freezing model, *Science Advances*, 8, eabq6842, <https://doi.org/10.1126/sciadv.abq6842>, 2022.
- Augustin-Bauditz, S., Wex, H., Kanter, S., Ebert, M., Niedermeier, D., Stolz, F., Prager, A., and Stratmann, F.: The immersion mode ice nucleation behavior of mineral dusts: A comparison of different pure and surface modified dusts, *Geophysical Research Letters*, 41, 7375–7382, <https://doi.org/10.1002/2014GL061317>, 2014.
- 520 Augustin-Bauditz, S., Wex, H., Denjean, C., Hartmann, S., Schneider, J., Schmidt, S., Ebert, M., and Stratmann, F.: Laboratory-generated mixtures of mineral dust particles with biological substances: Characterization of the particle mixing state and immersion freezing behavior, <http://dx.doi.org/10.34657/1057>, 2016.
- Baccarini, A., Karlsson, L., Dommen, J., Duplessis, P., Vüllers, J., Brooks, I. M., Saiz-Lopez, A., Salter, M., Tjernström, M., Baltensperger, U., Zieger, P., and Schmale, J.: Frequent new particle formation over the high Arctic pack ice by enhanced iodine emissions, *Nat Commun*, 11, 4924, <https://doi.org/10.1038/s41467-020-18551-0>, 2020.
- 525 Barry, K. R., Hill, T. C. J., Nieto-Caballero, M., Douglas, T. A., Kreidenweis, S. M., DeMott, P. J., and Creamean, J. M.: Active thermokarst regions contain rich sources of ice-nucleating particles, *Atmospheric Chemistry and Physics*, 23, 15783–15793, <https://doi.org/10.5194/acp-23-15783-2023>, 2023.
- 530 Beck, L. J., Sarnela, N., Junninen, H., Hoppe, C. J. M., Garmash, O., Bianchi, F., Riva, M., Rose, C., Peräkylä, O., Wimmer, D., Kausiala, O., Jokinen, T., Ahonen, L., Mikkilä, J., Hakala, J., He, X.-C., Kontkanen, J., Wolf, K. K. E., Cappelletti, D., Mazzola, M., Traversi, R., Petroselli, C., Viola, A. P., Vitale, V., Lange, R., Massling, A., Nøjgaard, J. K., Krejci, R., Karlsson, L., Zieger, P., Jang, S., Lee, K., Vakkari, V., Lampilahti, J., Thakur, R. C., Leino, K., Kangasluoma, J., Duplissy, E.-M., Siivola, E., Marbouti, M., Tham, Y. J., Saiz-Lopez, A., Petäjä, T., Ehn, M., Worsnop, D. R., Skov, H., Kulmala, M., Kerminen, V.-M., and Sipilä, M.: Differing Mechanisms of New Particle Formation at Two Arctic Sites, *Geophysical Research Letters*, 48, e2020GL091334, <https://doi.org/10.1029/2020GL091334>, 2021.
- 535 Berkemeier, T., Shiraiwa, M., Pöschl, U., and Koop, T.: Competition between water uptake and ice nucleation by glassy organic aerosol particles, *Atmospheric Chemistry and Physics*, 14, 12513–12531, <https://doi.org/10.5194/acp-14-12513-2014>, 2014.
- 540 Bigg, E. K.: Ice forming nuclei in the high Arctic, *Tellus B: Chemical and Physical Meteorology*, 48, 223–233, <https://doi.org/10.3402/tellusb.v48i2.15888>, 1996.
- Chi, J. W., Li, W. J., Zhang, D. Z., Zhang, J. C., Lin, Y. T., Shen, X. J., Sun, J. Y., Chen, J. M., Zhang, X. Y., Zhang, Y. M., and Wang, W. X.: Sea salt aerosols as a reactive surface for inorganic and organic acidic gases in the Arctic troposphere, *Atmospheric Chemistry and Physics*, 15, 11341–11353, <https://doi.org/10.5194/acp-15-11341-2015>, 2015.
- 545 Christiansen, S., Ickes, L., Bulatovic, I., Leck, C., Murray, B. J., Bertram, A. K., Wagner, R., Gorokhova, E., Salter, M. E., Ekman, A. M. L., and Bilde, M.: Influence of Arctic Microlayers and Algal Cultures on Sea Spray Hygroscopicity and the Possible Implications for Mixed-Phase Clouds, *Journal of Geophysical Research: Atmospheres*, 125, e2020JD032808, <https://doi.org/10.1029/2020JD032808>, 2020.

- 550 Creamean, J. M., Kirpes, R. M., Pratt, K. A., Spada, N. J., Maahn, M., de Boer, G., Schnell, R. C., and China, S.: Marine and terrestrial influences on ice nucleating particles during continuous springtime measurements in an Arctic oilfield location, *Atmospheric Chemistry and Physics*, 18, 18023–18042, <https://doi.org/10.5194/acp-18-18023-2018>, 2018.
- Creamean, J. M., Cross, J. N., Pickart, R., McRaven, L., Lin, P., Pacini, A., Hanlon, R., Schmale, D. G., Ceniceros, J., Aydele, T., Colombi, N., Bolger, E., and DeMott, P. J.: Ice Nucleating Particles Carried From Below a Phytoplankton Bloom to the Arctic Atmosphere, *Geophysical Research Letters*, 46, 8572–8581, <https://doi.org/10.1029/2019GL083039>, 2019.
- 555 Creamean, J. M., Barry, K., Hill, T. C. J., Hume, C., DeMott, P. J., Shupe, M. D., Dahlke, S., Willmes, S., Schmale, J., Beck, I., Hoppe, C. J. M., Fong, A., Chamberlain, E., Bowman, J., Scharien, R., and Persson, O.: Annual cycle observations of aerosols capable of ice formation in central Arctic clouds, *Nat Commun*, 13, 3537, <https://doi.org/10.1038/s41467-022-31182-x>, 2022.
- 560 DeMott, P. J., Prenni, A. J., Liu, X., Kreidenweis, S. M., Petters, M. D., Twohy, C. H., Richardson, M. S., Eidhammer, T., and Rogers, D. C.: Predicting global atmospheric ice nuclei distributions and their impacts on climate, *PNAS*, 107, 11217–11222, <https://doi.org/10.1073/pnas.0910818107>, 2010.
- 565 DeMott, P. J., Hill, T. C. J., McCluskey, C. S., Prather, K. A., Collins, D. B., Sullivan, R. C., Ruppel, M. J., Mason, R. H., Irish, V. E., Lee, T., Hwang, C. Y., Rhee, T. S., Snider, J. R., McMeeking, G. R., Dhaniyala, S., Lewis, E. R., Wentzell, J. J. B., Abbatt, J., Lee, C., Sultana, C. M., Ault, A. P., Axson, J. L., Diaz Martinez, M., Venero, I., Santos-Figueroa, G., Stokes, M. D., Deane, G. B., Mayol-Bracero, O. L., Grassian, V. H., Bertram, T. H., Bertram, A. K., Moffett, B. F., and Franc, G. D.: Sea spray aerosol as a unique source of ice nucleating particles, *Proceedings of the National Academy of Sciences*, 113, 5797–5803, <https://doi.org/10.1073/pnas.1514034112>, 2016.
- 570 Ebell, K., Buhren, C., Gierens, R., Chellini, G., Lauer, M., Walbröl, A., Dahlke, S., Krobot, P., and Mech, M.: Impact of weather systems on observed precipitation at Ny-Ålesund (Svalbard), *Atmospheric Chemistry and Physics*, 25, 7315–7342, <https://doi.org/10.5194/acp-25-7315-2025>, 2025.
- 575 Forster, P. M., Smith, C. J., Walsh, T., Lamb, W. F., Lamboll, R., Hauser, M., Ribes, A., Rosen, D., Gillett, N., Palmer, M. D., Rogelj, J., von Schuckmann, K., Seneviratne, S. I., Trewin, B., Zhang, X., Allen, M., Andrew, R., Birt, A., Borger, A., Boyer, T., Broersma, J. A., Cheng, L., Dentener, F., Friedlingstein, P., Gutiérrez, J. M., Gütschow, J., Hall, B., Ishii, M., Jenkins, S., Lan, X., Lee, J.-Y., Morice, C., Kadow, C., Kennedy, J., Killeck, R., Minx, J. C., Naik, V., Peters, G. P., Pirani, A., Pongratz, J., Schleussner, C.-F., Szopa, S., Thorne, P., Rohde, R., Rojas Corradi, M., Schumacher, D., Vose, R., Zickfeld, K., Masson-Delmotte, V., and Zhai, P.: Indicators of Global Climate Change 2022: annual update of large-scale indicators of the state of the climate system and human influence, *Earth System Science Data*, 15, 2295–2327, <https://doi.org/10.5194/essd-15-2295-2023>, 2023.
- 580 Fraund, M., Park, T., Yao, L., Bonanno, D., Pham, D. Q., and Moffet, R. C.: Quantitative capabilities of STXM to measure spatially resolved organic volume fractions of mixed organic&thinsp;&thinsp;inorganic particles, *Atmospheric Measurement Techniques*, 12, 1619–1633, <https://doi.org/10.5194/amt-12-1619-2019>, 2019.
- Fraund, M., Bonanno, D. J., China, S., Pham, D. Q., Veghte, D., Weis, J., Kulkarni, G., Teske, K., Gilles, M. K., Laskin, A., and Moffet, R. C.: Optical properties and composition of viscous organic particles found in the Southern Great Plains, *Atmospheric Chemistry and Physics Discussions*, 1–21, <https://doi.org/10.5194/acp-2020-255>, 2020.
- 585 Gong, X., Wex, H., van Pinxteren, M., Triesch, N., Fomba, K. W., Lubitz, J., Stolle, C., Robinson, T.-B., Müller, T., Herrmann, H., and Stratmann, F.: Characterization of aerosol particles at Cabo Verde close to sea level and at the cloud level – Part 2: Ice-nucleating particles in air, cloud and seawater, *Atmospheric Chemistry and Physics*, 20, 1451–1468, <https://doi.org/10.5194/acp-20-1451-2020>, 2020.

- 590 Gong, X., Zhang, J., Croft, B., Yang, X., Frey, M. M., Bergner, N., Chang, R. Y.-W., Creamean, J. M., Kuang, C., Martin, R. V., Ranjithkumar, A., Sedlacek, A. J., Uin, J., Willmes, S., Zawadowicz, M. A., Pierce, J. R., Shupe, M. D., Schmale, J., and Wang, J.: Arctic warming by abundant fine sea salt aerosols from blowing snow, *Nat. Geosci.*, 16, 768–774, <https://doi.org/10.1038/s41561-023-01254-8>, 2023.
- Graversen, R. G. and Wang, M.: Polar amplification in a coupled climate model with locked albedo, *Clim Dyn*, 33, 629–643, <https://doi.org/10.1007/s00382-009-0535-6>, 2009.
- 595 Hartmann, M., Blunier, T., Brügger, S. o., Schmale, J., Schwikowski, M., Vogel, A., Wex, H., and Stratmann, F.: Variation of Ice Nucleating Particles in the European Arctic Over the Last Centuries, *Geophysical Research Letters*, 46, 4007–4016, <https://doi.org/10.1029/2019GL082311>, 2019.
- 600 Hartmann, M., Gong, X., Kecorius, S., van Pinxteren, M., Vogl, T., Welti, A., Wex, H., Zeppenfeld, S., Herrmann, H., Wiedensohler, A., and Stratmann, F.: Terrestrial or marine – indications towards the origin of ice-nucleating particles during melt season in the European Arctic up to 83.7°&thinsp;N, *Atmospheric Chemistry and Physics*, 21, 11613–11636, <https://doi.org/10.5194/acp-21-11613-2021>, 2021.
- Hartmann, S., Schrödner, R., Hassett, B. T., Hartmann, M., van Pinxteren, M., Fomba, K. W., Stratmann, F., Herrmann, H., Pöhlker, M., and Zeppenfeld, S.: Polysaccharides—Important Constituents of Ice-Nucleating Particles of Marine Origin, *Environ. Sci. Technol.*, 59, 5098–5108, <https://doi.org/10.1021/acs.est.4c08014>, 2025.
- 605 Hill, T. c. j., DeMott, P. j., Conen, F., and Möhler, O.: Impacts of Bioaerosols on Atmospheric Ice Nucleation Processes, in: *Microbiology of Aerosols*, John Wiley & Sons, Ltd, 195–219, <https://doi.org/10.1002/9781119132318.ch3a>, 2017.
- Hiranuma, N., Brooks, S. D., Moffet, R. C., Glen, A., Laskin, A., Gilles, M. K., Liu, P., Macdonald, A. M., Strapp, J. W., and McFarquhar, G. M.: Chemical characterization of individual particles and residuals of cloud droplets and ice crystals collected on board research aircraft in the ISDAC 2008 study, *Journal of Geophysical Research: Atmospheres*, 118, 6564–6579, <https://doi.org/10.1002/jgrd.50484>, 2013.
- 610 Hoose, C. and Möhler, O.: Heterogeneous ice nucleation on atmospheric aerosols: a review of results from laboratory experiments, *Atmos. Chem. Phys.*, 12, 9817–9854, <https://doi.org/10.5194/acp-12-9817-2012>, 2012.
- Huang, W. T. K., Ickes, L., Tegen, I., Rinaldi, M., Ceburnis, D., and Lohmann, U.: Global relevance of marine organic aerosol as ice nucleating particles, *Atmospheric Chemistry and Physics*, 18, 11423–11445, <https://doi.org/10.5194/acp-18-11423-2018>, 2018.
- 615 Ickes, L., Porter, G. C. E., Wagner, R., Adams, M. P., Bierbauer, S., Bertram, A. K., Bilde, M., Christiansen, S., Ekman, A. M. L., Gorokhova, E., Höhler, K., Kiselev, A. A., Leck, C., Möhler, O., Murray, B. J., Schiebel, T., Ullrich, R., and Salter, M. E.: The ice-nucleating activity of Arctic sea surface microlayer samples and marine algal cultures, *Atmospheric Chemistry and Physics*, 20, 11089–11117, <https://doi.org/10.5194/acp-20-11089-2020>, 2020.
- 620 Irish, V. E., Hanna, S. J., Willis, M. D., China, S., Thomas, J. L., Wentzell, J. J. B., Cirisan, A., Si, M., Leaitch, W. R., Murphy, J. G., Abbatt, J. P. D., Laskin, A., Girard, E., and Bertram, A. K.: Ice nucleating particles in the marine boundary layer in the Canadian Arctic during summer 2014, *Atmospheric Chemistry and Physics*, 19, 1027–1039, <https://doi.org/10.5194/acp-19-1027-2019>, 2019a.
- 625 Irish, V. E., Hanna, S. J., Xi, Y., Boyer, M., Polishchuk, E., Ahmed, M., Chen, J., Abbatt, J. P. D., Gosselin, M., Chang, R., Miller, L. A., and Bertram, A. K.: Revisiting properties and concentrations of ice-nucleating particles in the sea surface microlayer and bulk seawater in the Canadian Arctic during summer, *Atmospheric Chemistry and Physics*, 19, 7775–7787, <https://doi.org/10.5194/acp-19-7775-2019>, 2019b.

- Jahl, L. G., Brubaker, T. A., Polen, M. J., Jahn, L. G., Cain, K. P., Bowers, B. B., Fahy, W. D., Graves, S., and Sullivan, R. C.: Atmospheric aging enhances the ice nucleation ability of biomass-burning aerosol, *Science Advances*, 7, eabd3440, <https://doi.org/10.1126/sciadv.abd3440>, 2021.
- 630 Jayaweera, K. and Flanagan, P.: Investigations on biogenic ice nuclei in the Arctic atmosphere, *Geophysical Research Letters*, 9, 94–97, <https://doi.org/10.1029/GL009i001p00094>, 1982.
- J. Murray, B., O’Sullivan, D., D. Atkinson, J., and E. Webb, M.: Ice nucleation by particles immersed in supercooled cloud droplets, *Chemical Society Reviews*, 41, 6519–6554, <https://doi.org/10.1039/C2CS35200A>, 2012.
- 635 Kanji, Z. A., Ladino, L. A., Wex, H., Boose, Y., Burkert-Kohn, M., Cziczo, D. J., and Krämer, M.: Overview of Ice Nucleating Particles, *Meteorological Monographs*, 58, 1.1-1.33, <https://doi.org/10.1175/AMSMONOGRAPHS-D-16-0006.1>, 2017.
- Kanji, Z. A., Sullivan, R. C., Niemand, M., DeMott, P. J., Prenni, A. J., Chou, C., Saathoff, H., and Möhler, O.: Heterogeneous ice nucleation properties of natural desert dust particles coated with a surrogate of secondary organic aerosol, *Atmospheric Chemistry and Physics*, 19, 5091–5110, <https://doi.org/10.5194/acp-19-5091-2019>, 2019.
- 640 Kawana, K., Taketani, F., Matsumoto, K., Tobo, Y., Iwamoto, Y., Miyakawa, T., Ito, A., and Kanaya, Y.: Roles of marine biota in the formation of atmospheric bioaerosols, cloud condensation nuclei, and ice-nucleating particles over the North Pacific Ocean, Bering Sea, and Arctic Ocean, *Atmospheric Chemistry and Physics*, 24, 1777–1799, <https://doi.org/10.5194/acp-24-1777-2024>, 2024.
- Kilcoyne, A. L. D., Tyliczszak, T., Steele, W. F., Fakra, S., Hitchcock, P., Franck, K., Anderson, E., Harteneck, B., Rightor, E. G., Mitchell, G. E., Hitchcock, A. P., Yang, L., Warwick, T., and Ade, H.: Interferometer-controlled scanning transmission X-ray microscopes at the Advanced Light Source, *J Synchrotron Rad*, 10, 125–136, <https://doi.org/10.1107/S0909049502017739>, 2003.
- 645 Kirpes, R. M., Bonanno, D., May, N. W., Fraund, M., Barget, A. J., Moffet, R. C., Ault, A. P., and Pratt, K. A.: Wintertime Arctic Sea Spray Aerosol Composition Controlled by Sea Ice Lead Microbiology, *ACS Cent. Sci.*, 5, 1760–1767, <https://doi.org/10.1021/acscentsci.9b00541>, 2019.
- Knopf, D. A. and Forrester, S. M.: Freezing of Water and Aqueous NaCl Droplets Coated by Organic Monolayers as a Function of Surfactant Properties and Water Activity, *J. Phys. Chem. A*, 115, 5579–5591, <https://doi.org/10.1021/jp2014644>, 2011.
- Knopf, D. A., Alpert, P. A., and Wang, B.: The Role of Organic Aerosol in Atmospheric Ice Nucleation: A Review, *ACS Earth Space Chem.*, 2, 168–202, <https://doi.org/10.1021/acsearthspacechem.7b00120>, 2018.
- 655 Knopf, D. A., Barry, K. R., Brubaker, T. A., Jahl, L. G., K. A., L. J., Li, J., Lu, Y., Monroe, L. W., Moore, K. A., Rivera-Adorno, F. A., Saucedo, K. A., Shi, Y., Tomlin, J. M., Vepuri, H. S. K., Wang, P., Lata, N. N., Levin, E. J. T., Creamean, J. M., Hill, T. C. J., China, S., Alpert, P. A., Moffet, R. C., Hiranuma, N., Sullivan, R. C., Fridlind, A. M., West, M., Riemer, N., Laskin, A., DeMott, P. J., and Liu, X.: Aerosol–Ice Formation Closure: A Southern Great Plains Field Campaign, *Bulletin of the American Meteorological Society*, 1, 1–50, <https://doi.org/10.1175/BAMS-D-20-0151.1>, 2021.
- 660 Korolev, A., McFarquhar, G., Field, P. R., Franklin, C., Lawson, P., Wang, Z., Williams, E., Abel, S. J., Axisa, D., Borrmann, S., Crosier, J., Fugal, J., Krämer, M., Lohmann, U., Schlenzcek, O., Schnaiter, M., and Wendisch, M.: Mixed-Phase Clouds: Progress and Challenges, <https://doi.org/10.1175/AMSMONOGRAPHS-D-17-0001.1>, 2017.
- Lata, N. N., Zhang, B., Schum, S., Mazzoleni, L., Brimberry, R., Marcus, M. A., Cantrell, W. H., Fialho, P., Mazzoleni, C., and China, S.: Aerosol Composition, Mixing State, and Phase State of Free Tropospheric Particles and Their Role in Ice Cloud Formation, *ACS Earth Space Chem.*, 5, 3499–3510, <https://doi.org/10.1021/acsearthspacechem.1c00315>, 2021.
- 665

- Lata, N. N., Cheng, Z., Dexheimer, D., Zhang, D., Mei, F., and China, S.: Vertical Gradient of Size-Resolved Aerosol Compositions over the Arctic Reveals Cloud Processed Aerosol in-Cloud and above Cloud, *Environ. Sci. Technol.*, <https://doi.org/10.1021/acs.est.2c09498>, 2023.
- 670 Leck, C. and Svensson, E.: Importance of aerosol composition and mixing state for cloud droplet activation over the Arctic pack ice in summer, *Atmospheric Chemistry and Physics*, 15, 2545–2568, <https://doi.org/10.5194/acp-15-2545-2015>, 2015.
- Li, G., Wieder, J., Pasquier, J. T., Henneberger, J., and Kanji, Z. A.: Predicting atmospheric background number concentration of ice-nucleating particles in the Arctic, *Atmospheric Chemistry and Physics*, 22, 14441–14454, <https://doi.org/10.5194/acp-22-14441-2022>, 2022.
- 675 Li, G., Wilbourn, E. K., Cheng, Z., Wieder, J., Fagerson, A., Henneberger, J., Motos, G., Traversi, R., Brooks, S. D., Mazzola, M., China, S., Nenes, A., Lohmann, U., Hiranuma, N., and Kanji, Z. A.: Physicochemical characterization and source apportionment of Arctic ice-nucleating particles observed in Ny-Ålesund in autumn 2019, *Atmospheric Chemistry and Physics*, 23, 10489–10516, <https://doi.org/10.5194/acp-23-10489-2023>, 2023.
- Mazzola, M., Viola, A. P., Lanconelli, C., and Vitale, V.: Atmospheric observations at the Amundsen-Nobile Climate Change Tower in Ny-Ålesund, Svalbard, *Rend. Fis. Acc. Lincei*, 27, 7–18, <https://doi.org/10.1007/s12210-016-0540-8>, 2016.
- 680 Mehndiratta, L., Lyp, A. E., Slade, J. H., and Grassian, V. H.: Immersion ice nucleation of atmospherically relevant lipid particles, *Environ. Sci.: Atmos.*, 4, 1239–1254, <https://doi.org/10.1039/D4EA00066H>, 2024.
- Mirrielees, J. A., Kirpes, R. M., Costa, E. J., Porter, G. C. E., Murray, B. J., Lata, N. N., Boschi, V., China, S., Grannas, A. M., Ault, A. P., Matrai, P. A., and Pratt, K. A.: Marine aerosol generation experiments in the High Arctic during summertime, *Elementa: Science of the Anthropocene*, 12, 00134, <https://doi.org/10.1525/elementa.2023.00134>, 2024.
- 685 Moffet, R. C., Henn, T., Laskin, A., and Gilles, M. K.: Automated Chemical Analysis of Internally Mixed Aerosol Particles Using X-ray Spectromicroscopy at the Carbon K-Edge, *Anal. Chem.*, 82, 7906–7914, <https://doi.org/10.1021/ac1012909>, 2010a.
- Moffet, R. C., Tivanski, A. V., and Gilles, M. K.: Fundamentals and Applications in Aerosol Spectroscopy, Signorell, R., Reid, JP, Eds, 243–272, 2010b.
- 690 Moffet, R. C., Tivanski, A. V., and Gilles, M. K.: Scanning Transmission X-ray Microscopy: Applications in Atmospheric Aerosol Research, Lawrence Berkeley National Lab. (LBNL), Berkeley, CA (United States), 2011.
- Möhler, O., Benz, S., Saathoff, H., Schnaiter, M., Wagner, R., Schneider, J., Walter, S., Ebert, V., and Wagner, S.: The effect of organic coating on the heterogeneous ice nucleation efficiency of mineral dust aerosols, *Environ. Res. Lett.*, 3, 025007, <https://doi.org/10.1088/1748-9326/3/2/025007>, 2008.
- 695 Morrison, H., Shupe, M. D., Pinto, J. O., and Curry, J. A.: Possible roles of ice nucleation mode and ice nuclei depletion in the extended lifetime of Arctic mixed-phase clouds, *Geophysical Research Letters*, 32, <https://doi.org/10.1029/2005GL023614>, 2005.
- Morrison, H., de Boer, G., Feingold, G., Harrington, J., Shupe, M. D., and Sulia, K.: Resilience of persistent Arctic mixed-phase clouds, *Nature Geosci.*, 5, 11–17, <https://doi.org/10.1038/ngeo1332>, 2012.
- 700 Murray, B. J., Carslaw, K. S., and Field, P. R.: Opinion: Cloud-phase climate feedback and the importance of ice-nucleating particles, *Atmospheric Chemistry and Physics*, 21, 665–679, <https://doi.org/10.5194/acp-21-665-2021>, 2021.

- Patnaude, R. J., Moore, K. A., Perkins, R. J., Hill, T. C. J., DeMott, P. J., and Kreidenweis, S. M.: Low-temperature ice nucleation of sea spray and secondary marine aerosols under cirrus cloud conditions, *Atmospheric Chemistry and Physics*, 24, 911–928, <https://doi.org/10.5194/acp-24-911-2024>, 2024.
- 705 Prenni, A. J., Harrington, J. Y., Tjernström, M., DeMott, P. J., Avramov, A., Long, C. N., Kreidenweis, S. M., Olsson, P. Q., and Verlinde, J.: Can Ice-Nucleating Aerosols Affect Arctic Seasonal Climate?, *Bulletin of the American Meteorological Society*, 88, 541–550, <https://doi.org/10.1175/BAMS-88-4-541>, 2007.
- Quinn, P. K., Miller, T. L., Bates, T. S., Ogren, J. A., Andrews, E., and Shaw, G. E.: A 3-year record of simultaneously measured aerosol chemical and optical properties at Barrow, Alaska, *Journal of Geophysical Research: Atmospheres*, 107, AAC 8-1-AAC 8-15, <https://doi.org/10.1029/2001JD001248>, 2002.
- 710 Raif, E. N., Barr, S. L., Tarn, M. D., McQuaid, J. B., Daily, M. I., Abel, S. J., Barrett, P. A., Bower, K. N., Field, P. R., Carslaw, K. S., and Murray, B. J.: High ice-nucleating particle concentrations associated with Arctic haze in springtime cold-air outbreaks, *Atmospheric Chemistry and Physics*, 24, 14045–14072, <https://doi.org/10.5194/acp-24-14045-2024>, 2024.
- Rapp, C. N., Niu, S., Armstrong, N. C., Shen, X., Berkemeier, T., Surratt, J. D., Zhang, Y., and Cziczo, D. J.: Ice-nucleating properties of glassy organic and organosulfate aerosol, *Atmospheric Chemistry and Physics*, 25, 5519–5536, <https://doi.org/10.5194/acp-25-5519-2025>, 2025.
- 715 Rinaldi, M., Hiranuma, N., Santachiara, G., Mazzola, M., Mansour, K., Paglione, M., Rodriguez, C. A., Traversi, R., Becagli, S., Cappelletti, D., and Belosi, F.: Ice-nucleating particle concentration measurements from Ny-Ålesund during the Arctic spring–summer in 2018, *Atmospheric Chemistry and Physics*, 21, 14725–14748, <https://doi.org/10.5194/acp-21-14725-2021>, 2021.
- 720 Rogers, D. C., DeMott, P. J., and Kreidenweis, S. M.: Airborne measurements of tropospheric ice-nucleating aerosol particles in the Arctic spring, *Journal of Geophysical Research: Atmospheres*, 106, 15053–15063, <https://doi.org/10.1029/2000JD900790>, 2001.
- Rolph, G., Stein, A., and Stunder, B.: Real-time Environmental Applications and Display sYstem: READY, *Environmental Modelling & Software*, 95, 210–228, <https://doi.org/10.1016/j.envsoft.2017.06.025>, 2017.
- 725 Schill, G. P. and Tolbert, M. A.: Heterogeneous ice nucleation on phase-separated organic-sulfate particles: effect of liquid vs. glassy coatings, *Atmospheric Chemistry and Physics*, 13, 4681–4695, <https://doi.org/10.5194/acp-13-4681-2013>, 2013.
- Schmale, J., Sharma, S., Decesari, S., Pernov, J., Massling, A., Hansson, H.-C., von Salzen, K., Skov, H., Andrews, E., Quinn, P. K., Upchurch, L. M., Eleftheriadis, K., Traversi, R., Gilardoni, S., Mazzola, M., Laing, J., and Hopke, P.: Pan-Arctic seasonal cycles and long-term trends of aerosol properties from 10 observatories, *Atmospheric Chemistry and Physics*, 22, 3067–3096, <https://doi.org/10.5194/acp-22-3067-2022>, 2022.
- 730 Schnell, R. C. and Vali, G.: Freezing nuclei in marine waters, *Tellus*, 27, 321–323, <https://doi.org/10.3402/tellusa.v27i3.9911>, 1975.
- Screen, J. A. and Simmonds, I.: The central role of diminishing sea ice in recent Arctic temperature amplification, *Nature*, 464, 1334–1337, <https://doi.org/10.1038/nature09051>, 2010.
- 735 Serreze, M. C. and Barry, R. G.: Processes and impacts of Arctic amplification: A research synthesis, *Global and Planetary Change*, 77, 85–96, <https://doi.org/10.1016/j.gloplacha.2011.03.004>, 2011.

- Stein, A. F., Draxler, R. R., Rolph, G. D., Stunder, B. J. B., Cohen, M. D., and Ngan, F.: NOAA's HYSPLIT Atmospheric Transport and Dispersion Modeling System, <https://doi.org/10.1175/BAMS-D-14-00110.1>, 2015.
- 740 Stohl, A., Forster, C., Frank, A., Seibert, P., and Wotawa, G.: Technical note: The Lagrangian particle dispersion model FLEXPART version 6.2, *Atmospheric Chemistry and Physics Discussions*, 5, 4739–4799, 2005.
- Storelvmo, T.: Aerosol Effects on Climate via Mixed-Phase and Ice Clouds, *Annual Review of Earth and Planetary Sciences*, 45, 199–222, <https://doi.org/10.1146/annurev-earth-060115-012240>, 2017.
- 745 Tang, M., Cziczo, D. J., and Grassian, V. H.: Interactions of Water with Mineral Dust Aerosol: Water Adsorption, Hygroscopicity, Cloud Condensation, and Ice Nucleation, *Chem. Rev.*, 116, 4205–4259, <https://doi.org/10.1021/acs.chemrev.5b00529>, 2016.
- Tobo, Y.: *Sci Rep*, 6, 32930, <https://doi.org/10.1038/srep32930>, 2016.
- 750 Tunved, P., Ström, J., and Krejci, R.: Arctic aerosol life cycle: linking aerosol size distributions observed between 2000 and 2010 with air mass transport and precipitation at Zeppelin station, Ny-Ålesund, Svalbard, *Atmospheric Chemistry and Physics*, 13, 3643–3660, <https://doi.org/10.5194/acp-13-3643-2013>, 2013.
- Vali, G., DeMott, P. J., Möhler, O., and Whale, T. F.: Technical Note: A proposal for ice nucleation terminology, *Atmospheric Chemistry and Physics*, 15, 10263–10270, <https://doi.org/10.5194/acp-15-10263-2015>, 2015.
- 755 Vepuri, H. S. K., Rodriguez, C. A., Georgakopoulos, D. G., Hume, D., Webb, J., Mayer, G. D., and Hiranuma, N.: Ice-nucleating particles in precipitation samples from the Texas Panhandle, *Atmospheric Chemistry and Physics*, 21, 4503–4520, <https://doi.org/10.5194/acp-21-4503-2021>, 2021.
- Wagner, R., Ickes, L., Bertram, A. K., Els, N., Gorokhova, E., Möhler, O., Murray, B. J., Umo, N. S., and Salter, M. E.: Heterogeneous ice nucleation ability of aerosol particles generated from Arctic sea surface microlayer and surface seawater samples at cirrus temperatures, *Atmospheric Chemistry and Physics*, 21, 13903–13930, <https://doi.org/10.5194/acp-21-13903-2021>, 2021.
- 760 Wagner, R., Hu, Y., Bogert, P., Höhler, K., Kiselev, A., Möhler, O., Saathoff, H., Umo, N., and Zanatta, M.: How Porosity Influences the Heterogeneous Ice Nucleation Ability of Secondary Organic Aerosol Particles, *Journal of Geophysical Research: Atmospheres*, 129, e2024JD041576, <https://doi.org/10.1029/2024JD041576>, 2024.
- 765 Welti, A., Bigg, E. K., DeMott, P. J., Gong, X., Hartmann, M., Harvey, M., Henning, S., Herenz, P., Hill, T. C. J., Hornblow, B., Leck, C., Löffler, M., McCluskey, C. S., Rauker, A. M., Schmale, J., Tatzelt, C., van Pinxteren, M., and Stratmann, F.: Ship-based measurements of ice nuclei concentrations over the Arctic, Atlantic, Pacific and Southern oceans, *Atmospheric Chemistry and Physics*, 20, 15191–15206, <https://doi.org/10.5194/acp-20-15191-2020>, 2020.
- 770 Wendisch, M., Macke, A., Ehrlich, A., Lüpkes, C., Mech, M., Chechin, D., Dethloff, K., Velasco, C. B., Bozem, H., Brückner, M., Clemen, H.-C., Crewell, S., Donth, T., Dupuy, R., Ebell, K., Egerer, U., Engelmann, R., Engler, C., Eppers, O., Gehrman, M., Gong, X., Gottschalk, M., Gourbeyre, C., Griesche, H., Hartmann, J., Hartmann, M., Heinold, B., Herber, A., Herrmann, H., Heygster, G., Hoor, P., Jafariserajehlou, S., Jäkel, E., Järvinen, E., Jourdan, O., Kästner, U., Kecorius, S., Knudsen, E. M., Köllner, F., Kretzschmar, J., Lelli, L., Leroy, D., Maturilli, M., Mei, L., Mertes, S., Mioche, G., Neuber, R., Nicolaus, M., Nomokonova, T., Notholt, J., Palm, M., Pinxteren, M. van, Quaas, J., Richter, P., Ruiz-Donoso, E., Schäfer, M., Schmieder, K., Schnaiter, M., Schneider, J., Schwarzenböck, A., Seifert, P., Shupe, M. D., Siebert, H., Spreen, G., Stapf, J., Stratmann, F., Vogl, T., Welti, A., Wex, H., Wiedensohler, A., Zanatta, M., and Zeppenfeld, S.: The Arctic Cloud Puzzle: Using ACLOUD/PASCAL Multiplatform Observations to Unravel the Role of Clouds and Aerosol Particles in Arctic Amplification, <https://doi.org/10.1175/BAMS-D-18-0072.1>, 2019.
- 775

- 780 Wilbourn, E. K., Lacher, L., Guerrero, C., Vepuri, H. S. K., Höhler, K., Nadolny, J., Pantoya, A. D., Möhler, O., and Hiranuma, N.: Measurement report: A comparison of ground-level ice-nucleating-particle abundance and aerosol properties during autumn at contrasting marine and terrestrial locations, *Atmospheric Chemistry and Physics*, 24, 5433–5456, <https://doi.org/10.5194/acp-24-5433-2024>, 2024.
- 785 Wilson, T. W., Ladino, L. A., Alpert, P. A., Breckels, M. N., Brooks, I. M., Browse, J., Burrows, S. M., Carslaw, K. S., Huffman, J. A., Judd, C., Kilhau, W. P., Mason, R. H., McFiggans, G., Miller, L. A., Nájera, J. J., Polishchuk, E., Rae, S., Schiller, C. L., Si, M., Temprado, J. V., Whale, T. F., Wong, J. P. S., Wurl, O., Yakobi-Hancock, J. D., Abbatt, J. P. D., Aller, J. Y., Bertram, A. K., Knopf, D. A., and Murray, B. J.: A marine biogenic source of atmospheric ice-nucleating particles, *Nature*, 525, 234–238, <https://doi.org/10.1038/nature14986>, 2015.
- Xue, J., Zhang, T., Park, K., Yan, J., Yoon, Y. J., Park, J., and Wang, B.: Diverse sources and aging change the mixing state and ice nucleation properties of aerosol particles over the western Pacific and Southern Ocean, *Atmospheric Chemistry and Physics*, 24, 7731–7754, <https://doi.org/10.5194/acp-24-7731-2024>, 2024.
- 790 Zhao, X., Liu, X., Burrows, S. M., and Shi, Y.: Effects of marine organic aerosols as sources of immersion-mode ice-nucleating particles on high-latitude mixed-phase clouds, *Atmospheric Chemistry and Physics*, 21, 2305–2327, <https://doi.org/10.5194/acp-21-2305-2021>, 2021.
- Zobrist, B., Marcolli, C., Pedernera, D. A., and Koop, T.: Do atmospheric aerosols form glasses?, *Atmospheric Chemistry and Physics*, 8, 5221–5244, <https://doi.org/10.5194/acp-8-5221-2008>, 2008.